Project title: ***Hyperbranched Epoxy Nanohybrids Immobilized Natural Biocide for Advanced Marine Coatings***

Name of PI:	Prof. Niranjan Karak
Institution:	Tezpur University
Duration of project:	3 years
Date of commencement:	April 2012
Research fellow (**Names):**	Two (Shaswat Barua &Bibekananda De)
Specific application of the work:	Advanced marine coatings

Objectives of the project

The main objective of the proposed project is to develop a special type of antifouling coating for marine application. This objective is associated with the following sub-objectives.

1. To synthesize and characterize hyperbranched epoxy resins from multifunctional polyols like triethanol amine, poly(ε-caprolactone) diol, pentaerythitol, glycerol, bisphenol, hyperbranched polyol, etc. and epichlorohydrin.
2. To study the curing behavior of the resins with hyperbranched polyamines as well as conventional hardener systems.
3. To prepare epoxy/nanoclay and nanometals (such as Cu, Ag, etc. as they may exhibit antifouling property) nanohybrids.
4. To immobilize natural biocide such as biocidin / curcumin (for antifouling property) by the nanohybids and to study their releasing rate spectrophotometrically. The same will be compared with a standard synthetic biocide like Metdetomidine based system for comparison.
5. To characterize the prepared nanohybrid immobilized biocide systems by different analytical and instrumental techniques.
6. To study the performance characteristics of the nanohybrids as marine-coating materials with and without biocide. The final field test will be conducted by help of NRML, Thane in collaboration with NRB representative.
7. To study optimization conditions to obtain the best performance of the nanohybride immobilized biocides.

Work Done (Point wise till date v/s objectives)

For objective 1: Synthesis and characterization of a few hyperbranched epoxy resins are completed.

The epoxy resins were synthesized by A_2 + B_n polycondensation reaction, where A_2 is '*in situ*' generated diglycidyl ether of bisphenol-A and B_n is the 'n' number hydroxyl group containing polyol. One example we have shown in Scheme 1 from our last published work. The hyperbranched structures of the resins were confirmed by NMR study (Figure. 1). The NMR spectroscopy is an important tool for the characterization of degree of branching (DB) of a hyperbranched polymer. The DB is the ratio of the sum of integration of dendritic and terminal units to the sum of integration of dendritic, linear and terminal units, i.e., DB = (D + T)/(D + L + T). The epoxy protons were observed in the ^{1}H NMR spectrum (Figure 1 a) at δ = 2.7 ppm, 2.9 ppm for –CH_2 and 3.3 ppm for –CH. The degree of branching of the resins was calculated from ^{13}C NMR (Figure 1 b) and its range 0.5-0.8. The degree of branching of the resins was mainly depended on the mole ratio of the reactants and conditions of the reaction. Therefore the physical properties like epoxy equivalent, hydroxyl value, viscosity, etc. were also changed with these factors (Table 1). The resins were soluble most of the organic solvents like ethanol, methanol, acetone, THF, DMSO, DMAc, DMF, $CHCl_3$, CH_2Cl_2, toluene, xylene, etc. due to the presence of large number of functionality with hyperbranched architecture.

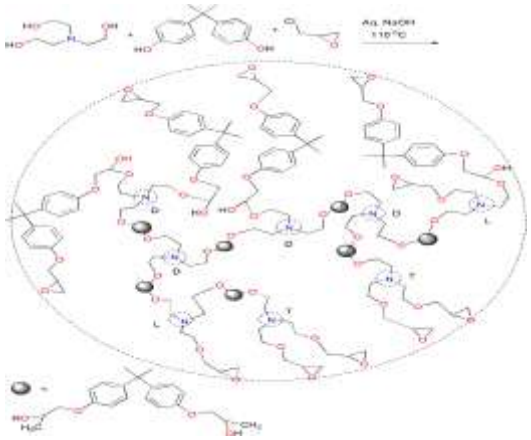

Scheme 1 Synthesis of hyperbranched epoxy

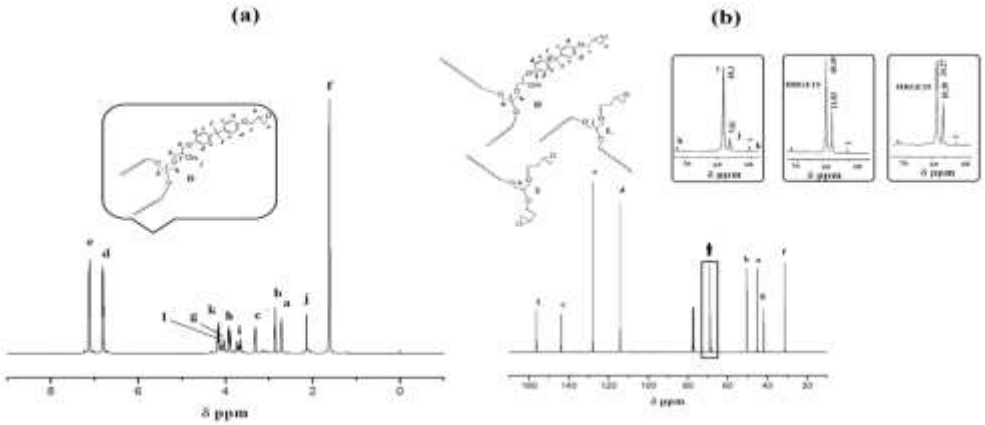

Figure 1 (a) ^{1}H-NMR spectrum and (b) ^{13}C-NMR spectrum of the hyperbranched epoxy resin

Table 1 Physical property of the resins

Properties	Value
Epoxy equivalent (g/eq.)	350-600
Hydroxyl value (mg KOH/g)	100-150
Viscosity (Pas) at 40 °C	10-25
Degree of branching (DB)	0.5-0.8
Curing time at 100 °C (min)	30-60
Post curing time at 130 °C (min)	15-30
Swelling value (%)	20-25

For objective 2: Curing behavior of the resins are studied with conventional and dendritic poly(amido amine) hardener systems. Various properties such as physical, mechanical, adhesive strength, thermal, chemical, etc. of the prepared thermosets were studied.

Curing of the hyperbranched epoxy resin was done at 100 -120°C with poly(amido amine) as the hardener and followed by post curing at 130 °C for specified time to obtain the desired swelling values (Table 1). The curing of the resins with hyperbranched polyamine (PAD) was done at room temperature by mixing with poly(amido-amine) as only hyperbranched polyamine cured thermosets showed brittle character (Table 2).

Table 2 Amount of hardener, curing time and swelling value of the thermosets

Thermosets	Amount of hardener (%)		Curing time at 25 °C (h)		Swelling value at 25 °C (%)
	Poly(amido-amine)	PAD	Touch free	Hard cure	
PAD0	50	0	8	72	41 [a]
PAD5	20	5	2	9	27
PAD10	20	10	1	6	15
PAD15	20	15	0.75	5	18
OPAD	0	20	0.5	3	11

[a] The swelling value of PAD0 was 16 % while cured at 100 °C

Performance of the thermosets are given in Table 3 and Table 4 after curing with poly(amido-amine) and combine hardener respectively. Chemical resistance of the thermosets in different chemical environments is given in Table 5.

Table 3 Performance of the thermosets

Properties	Value
Tensile strength (MPa)	20-50
Elongation at break (%)	25-50
Toughness	800-1300
Scratch hardness (kg)	8.0-9.5
Impact strength (cm)[a]	>100
Bending dia. (mm)[b]	<1
Gloss at 60 °C	110-130
Adhesion strength (M-M) (MPa)	1500-3000
Adhesion strength (W-W) (MPa)[c]	700-1300
Initial degradation temperature (°C)	300
Mid-point degradation temperature (°C)	400
Weight residue (%) at 600 °C	10-20

[a] The limit of the impact strength was 100 cm (highest), [b] The limit of the mandrel diameter was 1 mm (lowest), [c] In all the thermosets plywood substrate was failed

Table 4 Performance of the thermosets

Properties	PAD0	PAD5	PAD10	PAD15	OPAD
Tensile strength (MPa)	47	51	70	62	-
Elongation at break (%)	21	19	14	16	-
Toughness [a] (MPa)	413	396	438	400	-
Scratch hardness [b] (kg)	9.0	9.0	>10.0	9.5	5.0
Impact strength [c] (cm)	>100	95	95	90	60
W-W, lap-shear tensile strength [d] (MPa)	2300	>3941	>4226	>4029	>4256
M-M, lap-shear tensile strength (MPa)	2662	5688	6064	5964	7257
Dielectric constant at 1 MHz (at 20 °C)	3.16	3.22	3.26	3.32	-
Dielectric loss at 1 MHz (at 20 °C)	0.010	0.012	0.013	0.014	-
Moisture absorption at 25 °C (%)	0.85	0.43	0.11	0.19	0.08
Thermal stability (°C)	298	286	295	296	-

[a] Measured by integrating the stress-strain curves, [b] The limit of the scratch hardness was 10.0 kg, [c] The limit of the impact strength was 100 cm, [d] In all the combine hardener cured thermosets and OPAD wood substrates were failed.

Table 5 Weight loss (%) of the thermosets in different chemical environment after 30 days

Chemical environments	Value
Aq. HCl (10%)	0.90-1.0
Aq. NaOH (5%)	1.0-2.0
Aq. NaCl (15%)	0.2-0.5
Aq. EtOH (20%)	NC[a]
Pure water	NC

[a] NC = no weight change

For objective 3: Different nanomaterials like Ag, Cu-oxides, modified clay, carbon dot, carbon dot reduced Cu_2O nanohybrid, etc are prepared for preparation of epoxy nanocomposites. Performance of the hyperbranched epoxy/modified clay and hyperbranched epoxy carbon dot nanocomposites is given in Table 7 and 8. The stress-strain profiles of the clay-silver nanocomposites with hyperbranched epoxy are presented in Figure 5.

Ag nanoparticles and their nanocomposites with hyperbranched epoxy

Ag nanoparticles were prepared by using the aqueous leaf extract of *Colocasia esculenta* and *Thuja occidentalis*. The prepared metal nanoparticles were characterized by UV–visible spectroscopy and XRD (Figure 2a). These were distributed within a narrow size spectrum of (12-14 nm) as revealed by transmission electron microscopic imaging (Figure 2b). Antimicrobial potency of the prepared particles was tested against both gram positive and gram-negative bacteria (Figure 3). The prepared nanoparticles were found to be eco-compatible as tested on the earthworm species *Eisenia fetida* (Table 6).

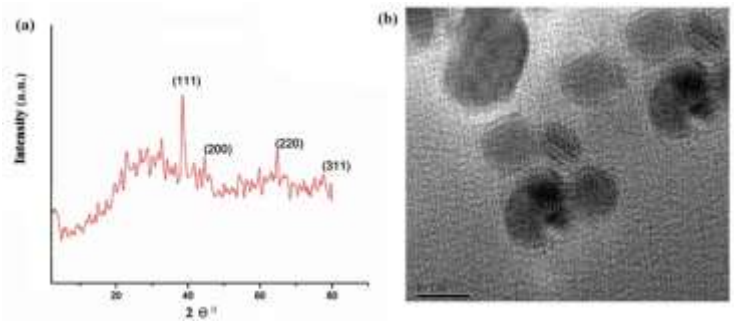

Figure 2 (a) XRD-pattern and (b) TEM image of silver nanoparticles

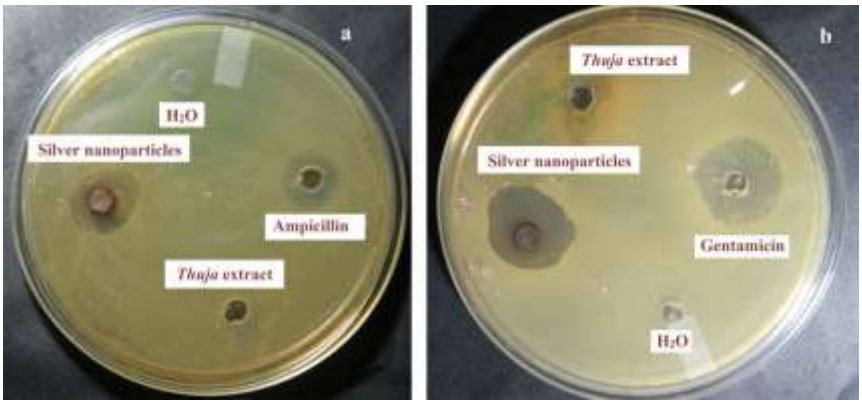

Figure 3 Antibacterial activities of the prepared silver nanoparticles, for (a) *S. aureus* and (b) *E. coli*.

Table 6 Count of earthworm and cocoon production on application of silver nanoparticles

Count	Control	Concentration of silver nanoparticles (ppm)						
		50	150	200	250	500	1000	*P* value
Earthworm	14±0.57	14±1.53	15±1.53	17±1.53	18±0.57	20±0.57	21±0.57	0.002
Cocoon	4±1.00	4±1.00	6±1.00	7±0.57	9±1.53	9±0.57	11±1.53	0.003

UV-visible spectra showed the formation of silver nanoparticles (Figure 4a). Morphology of the clay/silver nanohybrid was studied by transmission electron microscopy (TEM, Figure 4b). However, the intensity decreased upon preparation of the nanohybrid.

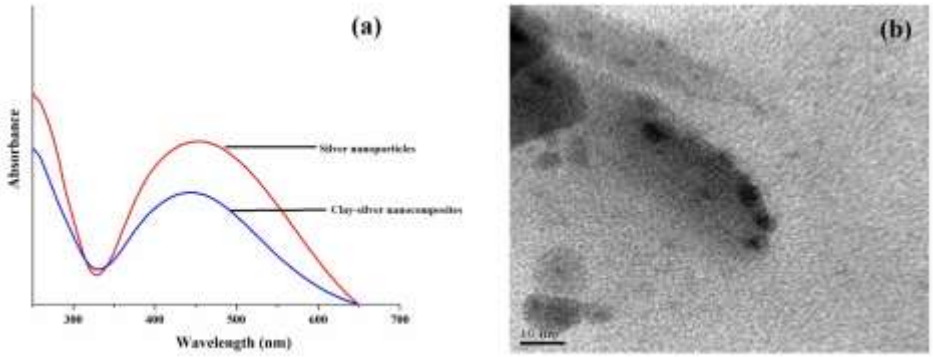

Figure 4 (a) UV-visible spectra and (b) TEM image of the prepared nanohybrid

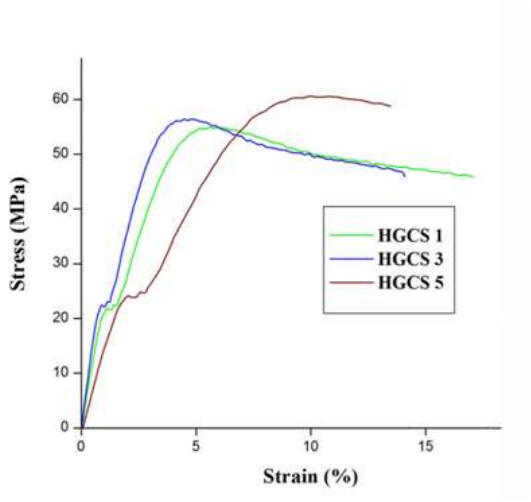

Figure 5 Stress-strain profiles of clay-silver nanocomposites

Hyperbranched epoxy nanocomposites with modified bentonite clay

The hydrophilic bentonite clay was modified by alkyl ammonium moiety by ion exchange process. Na^+ ions of hydrophilic bentonite clay were exchanged by aliphatic first generation poly(amido-ammonium) ion. The characteristic diffraction peak shifted from 2θ = 7.1 ° to 4.9 ° after modification (Figure 6a). Thus basal spacing increases 0.56 nm after modification as calculated from XRD data by Bragg's equation. This is due to the fact that the clay layers are intercalated by the branched structure of poly(amido-amine) modifying agent. The nanocomposites were prepared by solution technique with the help of mechanical shearing and sonication with 1, 3 and 5 wt% modified clay and coded as MNC1, MNC3 and MNC5 respectively. The curing time of the nanocomposites with 50% poly(amido-amine) at 100 °C decreases with the increases of clay content in the nanocomposites (Table 7). This is due to the strong interaction of hyperbranched epoxy with the modified clay. The aliphatic poly(amido-amine) of the clay also took part in crosslinking reaction with the hyperbranched epoxy. The diffraction peak for d_{001} of the modified clay at 2θ = 4.9° was completely diminished in nanocomposites as observed in XRD patterns (Figure 6b). This may be due to the intercalation of polymer chain into the clay layers and also strong interactions like hydrogen bonding, polar-polar interactions, etc. which facilitate the well dispersions of clay layers with the epoxy. The TEM image discloses the actual picture of state of dispersion of clay in the nanocomposites. Figure 7a reveals the homogenous dispersion of disordered structure of clay layers in the epoxy matrix. The image shows both the exfoliation and intercalation of clay layers in hyperbranched epoxy matrix. SEM is also a valuable technique for examining the morphology of the nanocomposites. Uniform dispersion of clay in the hyperbranched epoxy was also confirmed by the SEM image of the fracture surface of the nanocomposite (Figure 7b). This uniform dispersion is due to the strong phisico-chemical interactions of aliphatic poly(amido-amine) of modified clay with hyperbranched epoxy and the hardener.

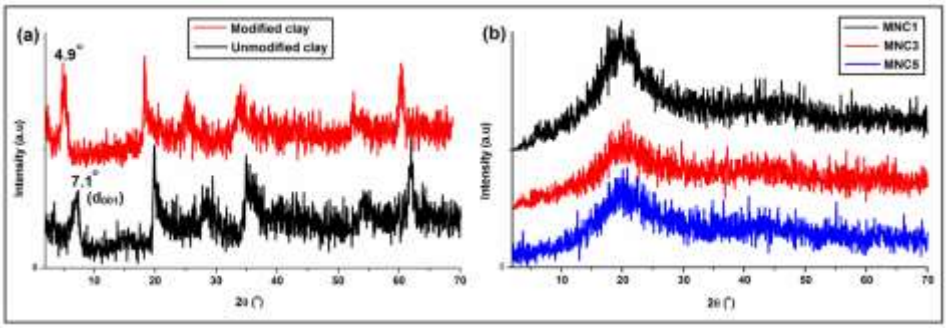

Figure 6 (a) XRD patterns of pristine and modified bentonite and (b) XRD patterns of nanocomposites

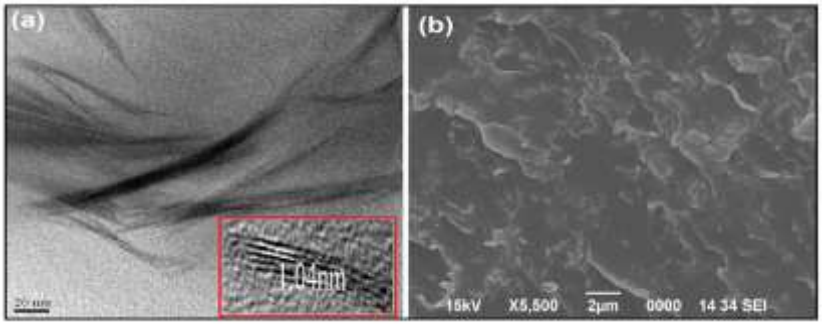

Figure 7 (a) TEM and (b) SEM images of MNC3

The mechanical properties of the nanocomposites with different amount of clay loading were given in the Table 7. The interesting results in this study were the achievement of excellent toughness and high flexibility of the nanocomposites. The toughness of the nanocomposites as determined by integrating the stress-strain curves was sharply increased with the increase of amount of clay and thus the nanocomposites behave like ductile materials. This is the combined effects of the flexible hydrocarbon chains of the aliphatic branched poly(amido-amine), the modifying agent; different flexible moieties of hyperbranched epoxy and the long chain hydrocarbon part of the fatty acid of poly(amido-amine) hardener with the aromatic rigid moiety and clay platelets. The plasticizing effect of these flexible moieties has definite role for the above results. Again, both hyperbranched epoxy and branched poly(amido-amine) help to increase the free volume between the molecules because of the steric effect . It is also possible that clay platelets act as both physical and chemical crosslinkers. Both platelet motion and long range intercalations through physical crosslinks are potential candidates for the observed toughening of hyperbranched epoxy. The elongation at break was sharply increased with the increase of the amount of clay loading. The tensile strength of the nanocomposites also increased with the increase of amount of clay content. At higher clay loading (5%) agglomeration of clay particles in the polymer matrix discontinues the increment of the tensile strength of the nanocomposite. The impact strength and scratch hardness were also very high for the nanocomposites. The nanocomposites were exhibited high flexibility as they bent up to the lowest diameter of a

mandrel (1 mm) or 180° without any damage or fracture for the same reason. As both the nanocomposites and the pristine epoxy were crossed the highest limit of the impact resistance (100 cm) and flexibility (1 mm), the enhancement of these values could not determine. The nanocomposites were also crossed the highest limit (Instrument) of the scratch hardness value (10.0 kg).

Two fold improvement in adhesive strength with both wood-wood (W-W) and metal-metal (M-M) substrates was found after formation of nanocomposites (Table 7). This is due to the presence of highly polar oxygen and nitrogen containing groups of epoxy, hardener and clay, which help to generate strong interaction with the cellulosic wood substrates. The diffusion of clay dispersed hyperbranched epoxy and hardener into the metal substrates helps to strong physical interlocking.

Table 7 Performance of the nanocomposites

Properties	MNC1	MNC3	MNC5	BNC3 [e]
Curing time at 100 °C (min)	70-75	52-57	43-47	88-92
Swelling value (%) at 25 °C	19-21	21-22	22-24	30-35
Tensile strength (MPa)	45-47	56-59	40-42	17-19
Elongation at break (%)	31-33	42-44	54-55	55-57
Toughness	830-838	1800-1810	1626-1630	820-830
Impact resistance [a] (cm)	>100	>100	>100	95
Scratch hardness [b] (kg)	>10.0	>10.0	>10.0	8.5
Bending dia. [c] (mm)	<1	<1	<1	<1
Adhesive strength [d] (W-W) (MPa)	>4348	>4393	>4414	>3422
Adhesive strength (M-M) (MPa)	6690-6700	6740-6750	6750-6760	3650-3660

[a] *The limit of the impact strength was 100 cm (highest),* [b] *The limit of the scratch hardness was 10.0 kg (highest),* [c] *The limit of the mandrel diameter was 1 mm (lowest),* [d] *In all the nanocomposites wood substrate was failed,* [e] *BNC3 is the hyperbranched epoxy nanocomposite with 3 wt% unmodified bentonite clay.*

Carbon dot and its nanocomposites with hyperbranched epoxy

Carbon dots were prepared by simply heating banana juice in a glass bottle. An amount of 20 mL of the juice (pulp-free, solid content 52 mg/mL) was taken with 20 mL of ethanol in a 60 mL glass bottle plugged with cotton cork and heated at constant temperature of 150 °C in an oven for 4 h. The dark brown product was obtained after cooling at room temperature. This was filtrated and centrifuged at 960 g (3000 rpm) for 15 min under ambient conditions to separate the large particles. The yield of the desired carbon dots was 600 mg (58% mass yield).

The formation of carbon dots with an average size 3 nm was confirmed from TEM micrographs as shown in Figure 8. The elemental compositions as the weight and atomic ratios of C and O of the carbon dots estimated from EDX data were 63.39:35.69 and 70.07:29.61 respectively. A minor amount of potassium was also found due to the use of banana resource, which contains this element. The different oxygenous functional groups and linkages in the carbon dots were evident by FTIR data (Figure 9a). In this spectrum stretching frequency at 3492, 2935, 1730, 1625, 1422, 1264 and 918 cm^{-1} indicated the presence of –OH, -C-H, C=O, C=C, C-O-C, C-O and epoxy ring respectively. The presence of these functional groups imparts excellent water solubility of the synthesized carbon dots. XRD pattern (Figure 9b) of the carbon dots showed a broad peak at 21.1°corresponds to the (002) peak. This indicated the interlayer spacing (d) of the carbon dots (0.42 nm) is higher than that of the graphitic interlayer spacing (0.33 nm) along with broadness character. This confirmed the enhancement of amorphous nature of carbon dots, which is attributed to the generation of more oxygen containing groups.

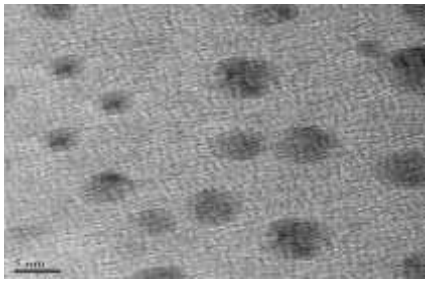

Figure 8 TEM image of carbon dots

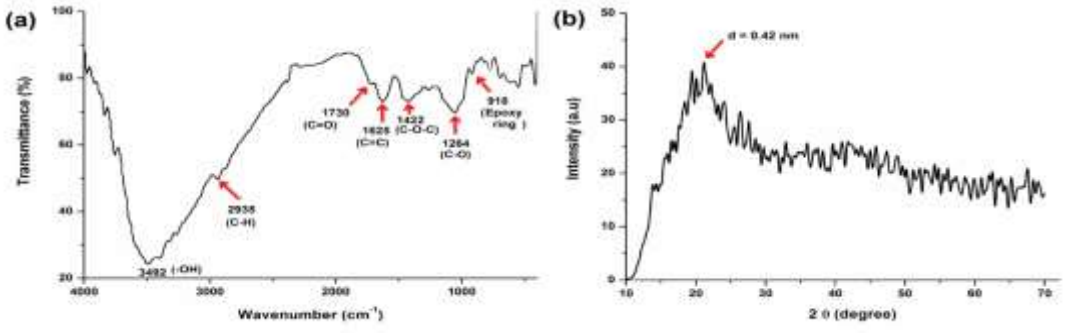

Figure 9 (a) FTIR and (b) XRD of carbon dot

The nanocomposites were prepared with the help of mechanical shearing and sonication with 0.1, 0.5 and 1.0 wt% carbon dot and coded as ECD0.1, ECD0.5 and ECD1.0 respectively. The curing time of the nanocomposites with 50 wt% poly(amido-amine) at 100 °C decreases with the increase of the amount of the carbon dots. This is due to the presence of large numbers of polar functional groups (like, hydroxy, epoxy, carbonyl, ether, etc. as revealed from FTIR spectrum) in carbon dots which

took part in crosslinking reaction and also resulted strong interfacial interaction with the hyperbranched epoxy matrix. The characteristics bands for the hyperbranched epoxy were observed at 3391, 2963, 1606, 1241, 1037 and 914 cm^{-1} for the presence of –OH, C-H, C=C, C-O, C-C and oxirane bands in the FTIR spectrum (Figure 10). The bands at 3492, 2935, 1730, 1625, 1422, 1264 and 915 cm^{-1} are attributed for –OH, C-H, C=O, C=C, C-O-C, C-O and oxirane linkages of the carbon dots as evident from Figure 10. In the FTIR spectrum of the nanocomposite, a broad band for –OH stretching frequency was observed at 3290 cm^{-1}. This shift compared to pristine polymer is due to the strong interaction and chemical crosslinking of carbon dots with the hyperbranched epoxy and hardener. The carbonyl peak of the carbon dots (1730 cm^{-1}) was also shifted to 1670 cm^{-1} after formation of nanocomposites. This is because of the formation of amide linkages by the reaction of carboxylic acid and ester groups of the carbon dots with the amino groups of hardener. The oxirane bands of the hyperbranched epoxy (914 cm^{-1}) and carbon dots (915 cm^{-1}) were completely vanished in the nanocomposite due to their participation in chemical crosslinking reaction.

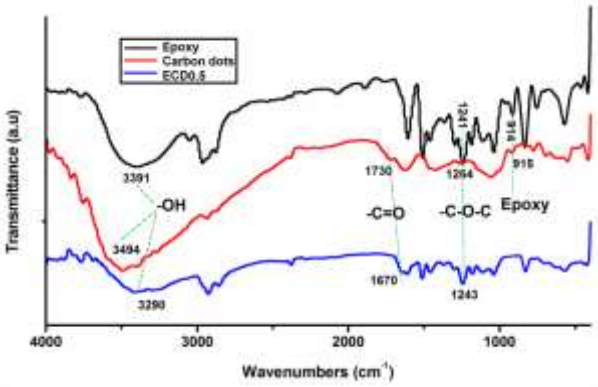

Figure 10 FTIR spectra of hyperbranched epoxy, carbon dot and nanocomposites

Excellent dispersion of carbon dots in the polymer matrix was supported by TEM micrograph (Figure 11) of ECD0.5 showing the carbon dots are well separated in the matrix without aggregation. The fine dispersion of the carbon dots is due to the chemical binding to the polymer matrix with large numbers of functional groups during the curing reaction preventing agglomeration. The internal spacing of the carbon dot was increased after formation of nanocomposite as shown in the inset picture of the TEM image.

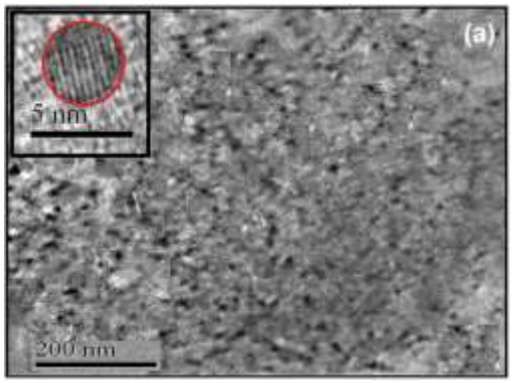

Figure 11 TEM image of ECD0.5

Mechanical properties like tensile strength, elongation at break, toughness, impact resistance, scratch hardness and bending of the nanocomposites are given in Table 8. However, the elongation at break and the toughness of the hyperbranched epoxide were dramatically enhanced after the formation of nanocomposites even at very low weight load of the carbon dots. The tensile strength and scratch hardness of the pristine epoxy were also improved by formation of the nanocomposites. The tensile strength increases with the increase of carbon dot content evident from stress-strain profiles (Figure 12). However, for ECD1.0 the tensile strength was lower than for ECD0.5. This is due to the small aggregations of carbon dots in the polymer matrix as shown in the TEM image of ECD1.0. The nanocomposites also exhibited high impact resistance and flexibility. Since both, the pristine hyperbranched epoxy thermoset as well as the nanocomposites reached the measurement limits of the instruments for impact resistance (100 cm), flexibility evaluation (1 mm), and scratch resistance (10.0 kg), the enhancement of these values by adding the carbon dots could not be determined. Clearly, these results indicate a dramatic enhancement of the toughness of the hyperbranched epoxy thermosets by the incorporation of a very low amount of carbon dots. The stress-strain profiles (Figure 10) also revealed the high improvement in elasticity of the epoxy thermoset by the formation of nanocomposites. This simultaneous improvement in strength, toughness **a**nd flexibility of the hyperbranched epoxy is a highly commendable achievement. This may be due to the presence of the aromatic carbonized core structure with highly polar surface functional groups in the carbon dots. This provides on the one hand a strong and stiff nanomaterial, which is enhancing mechanical properties of the polymer matrix, and on the other hand, a very strong physico-chemical interaction between the nano-filler and the matrix, which is further enhanced by the very small size of the carbon dots and thus, the huge surface area which interacts. The polar functional groups (like hydroxy, epoxy, carbonyl, ether, etc.) of the carbon dots took part in the physical and chemical crosslinking with the hyperbranched epoxy and the hardener.

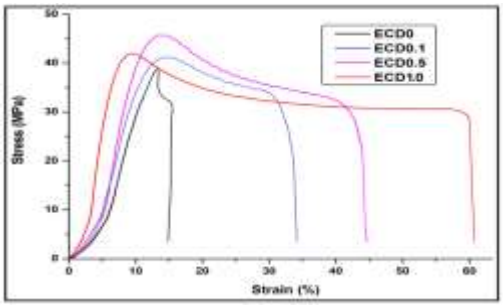

Figure 12 Stress-strain profiles of hyperbranched epoxy thermoset and nanocomposite

Table 8 Performance of the hyperbranched epoxy/carbon dot Nanocomposites.

Properties	ECD0.1	ECD0.5	ECD1.0
Curing at 100 ^{o}C (min)	60-62	44-46	40- 42
Swelling (%) at 25 ^{o}C	22-24	20-22	20-23
Tensile strength (MPa)	40-41	45-47	42-44
Elongation at break (%)	34-36	45-47	61-65
Toughness [a]	982-990	1452-1470	1889-1900
Impact strength (cm) [b]	>100	>100	>100
Scratch hardness (kg) [c]	>10.0	>10.0	>10.0
Bending dia. (mm) [d]	>1	>1	>1
Adhesive strength, W-W (MPa) [e]	>4680	>5678	>5686
Adhesive strength, M-M (MPa)	4270-4275	7060-7077	9130-9140

[a] Calculated by integrating the area under stress-strain curves, [b] The limit of the impact strength was 100 cm (highest), [c] The limit of the scratch hardness was 10.0 kg (highest), [d] The limit of the mandrel diameter was 1 mm (lowest), [e] In case of ECD0.5 and ECD1.0 wood substrates were failed.

In addition, two to three fold enhancements in adhesive strength for wood and metal substrates, respectively, were observed by the incorporation of only 1.0 wt% carbon dots into the hyperbranched epoxy thermoset (Table 8). This is due to the presence of polar functionalities in carbon dots which help to have strong interactions and physical interlocking with the substrates, and these increase with the increase of the amount of carbon dots in the thermoset. In case of ECD0.5 and ECD1.0 nanocomposites substrate failure was observed for wood and thus, they exhibited even higher adhesive strength than the reported values in Table 8. The different polar functional groups of

cellulosic wood substrate strongly interact with the polar functional groups present in the hyperbranched epoxy polymer, carbon dot and the hardener. For the metal substrate, however, strong physical interlocking with the hyperbranched epoxy and the different functional groups of carbon dots is the main reason for the high adhesive strength. The strong physical interlocking is due to the easy diffusion of low viscous hyperbranched epoxy and hardener along with the spherical fine particles of carbon dots into the surface structure of the metal substrate.

Carbon dot reduced Cu_2O nanohybrid and its nanocomposites with hyperbranched epoxy

The carbon dot reduced Cu_2O nanohybrid was prepared by the reduction of Cu^{2+} by carbon dot. Here, carbon dots act as reducing as well as capping agent. Carbon dots contain a large number of polar functional groups on their surface as revealed from FTIR of carbon dot. The peripheral hydroxyl and aldehyde groups of carbon dot help to reduce the Cu^{+2} into Cu^{+}. The hydroxyl groups reduce Cu^{2+} by polyphenolic mechanism and the aldehyde groups reduce Cu^{2+} as like Benedict test reaction. In FTIR spectra (Figure 13) it was found that the amount of hydroxyl groups (at 3400-3500 cm^{-1}) of carbon dot decreased after the formation of the carbon dot reduced Cu_2O nanohybrid, whereas the amount of carbonyl groups (at 1650 cm^{-1}) increased. This is because of the fact that the hydroxyl groups are converted into keto groups while aldehyde groups are converted into carboxylic acid groups. Other functional groups and chemical linkages of carbon dot remained constant after formation of the nanohybrid. The Cu-O bonds were found in FTIR spectrum of the nanohybrid at 465 and 556 cm^{-1}. The peripheral polar groups of carbon dot also stabilize the Cu_2O nanoparticles on their surface. The formation of the nanohybrid was confirmed by TEM images (Figure 14). The Figure 1a, reveals that the nanoparticles are nearly spherical in shape with average diameter of around 3-4 nm. From Figure 1a and 2a, it was confirmed that Cu_2O attached carbon dot and carbon dot embedded Cu_2O were formed. The formation of Cu_2O was confirmed from the XRD pattern of the nanohybrid (Figure 15). The crystallographic spacing d_{111}, d_{200}, d_{220} and d_{311} of Cu_2O were found at 2θ (°) = 36.4, 42.3, 61.4 and 73.5 respectively, which are comparable with the other reports of Cu_2O as well as JCPDF #78-2076 data. In the inset picture of TEM images (Figure 14a and b) two types of lattice spacing of 0.27 and 0.38 nm were found, which correspond to the d_{111} spacing of Cu_2O and d_{002} spacing of carbon dot, respectively.

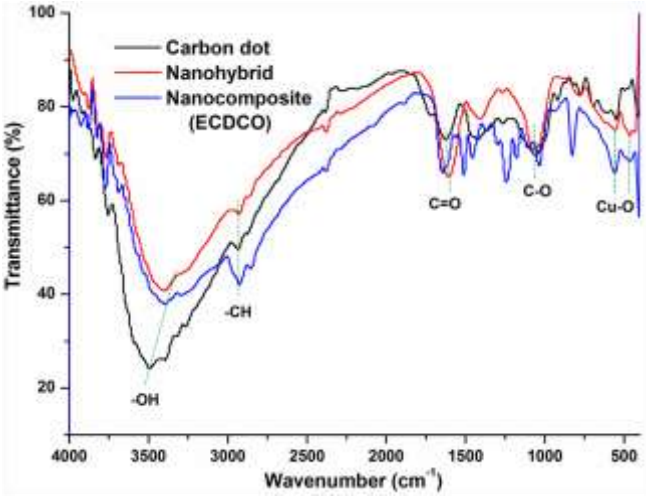

Figure 13 FTIR spectra of carbon dot, carbon dot reduced Cu_2O nanohybrid and ECDO

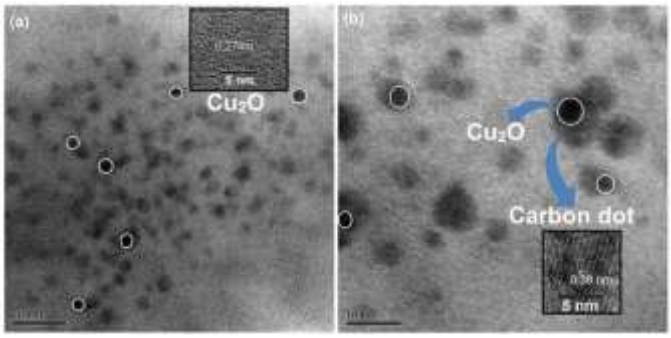

Figure 14 TEM images (a) 20 nm magnification (inset: the internal structure of Cu_2O), (b) 10 nm magnification (inset: the internal structure of carbon dot) carbon dot reduced Cu_2O nanohybrid

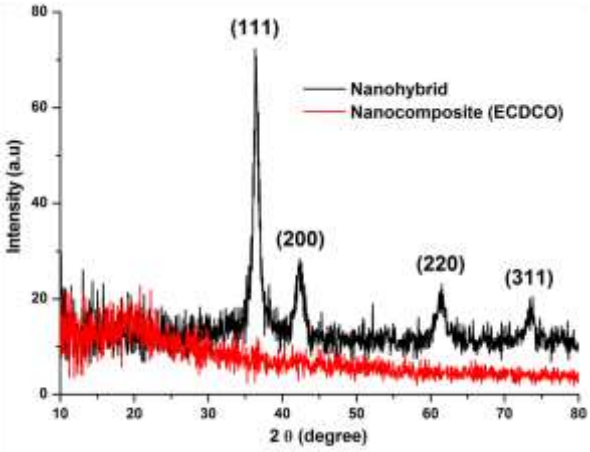

Figure 15 XRD patterns for carbon dot reduced Cu_2O nanohybrid and ECDCO

The nanocomposites were prepared by solution technique and cured with poly(amido-amine) hardener. The carbon dot/hyperbranched epoxy (ECD) was used here only for comparison purpose and it was already characterized in our earlier study. Carbon dot reduced Cu_2O nanohybrid/hyperbranched epoxy nanocomposites were coded as ECDCO0.5, ECDCO1.0 and

ECDCO1.5 with respect to 0.5, 1.0 and 1.5 wt% nanohybrid respectively. Nanocomposites were characterized by FTIR, XRD and TEM analyses. In the FTIR spectra (Figure 13) the hydroxyl band of carbon dot reduced Cu_2O nanohybrid shifted to 3390 from 3415 cm^{-1} after formation of the nanocomposite. This is due to the presence of different physico-chemical interactions of carbon dots and Cu_2O nanoparticles with the hyperbranched epoxy. Due to the same reason the Cu-O bands of nanohybrid also shifted to 558 and 468 cm^{-1} after formation of nanocomposite. The strong interaction of the nanoparticles with the hyperbranched epoxy matrix was also revealed from XRD patterns (Figure 15). The crystallographic peaks of the nanohybrid were completely diminished after formation of the nanocomposite whereas an amorphous polymeric peak at $2\theta = 20°$ was observed.

Mechanical properties like, tensile strength, elongation at break, toughness, impact resistance, scratch hardness and bending values of nanocomposites are given in Table 9. From the results it was found that tensile strength of pristine epoxy was improved up to 20% after formation of nanocomposite with 1.5 wt% nanohybrid. However, elongation at break and toughness of hyperbranched epoxy thermoset was increased dramatically by factors 2.5 and 3.5 folds after formation of nanocomposite with same amount of nanohybrid. The stress-strain profiles of pristine thermoset as well as its nanocomposites are shown in Figure 16. From the figure it can be found that tensile strength, elongation at break and toughness (area under stress-strain curves) of the hyperbranched epoxy thermoset increased with the increase of amount of nanohybrid loading. As toughness of hyperbranched epoxy thermoset was dramatically improved, the other mechanical properties like impact resistance and scratch hardness which were related to toughness were also improved by the formation of nanocomposites. However these differences could not be measured as the values for nanocomposites reached the highest limit of the instruments for scratch hardness (10 kg) and impact resistance (100 cm). Nanocomposites were also exhibited highest limit of the instrument for flexibility evaluation (1 mm bending diameter of mandrel) without damage of the film.

Table 9 Performance of pristine hyperbranched epoxy and its nanocomposites with carbon dot reduced Cu_2O nanohybrid

Parameters	ECDCO0.5	ECDCO1	ECDCO1.5
Swelling value (%)	24	23	21
Tensile strength (MPa)	43±1.5	45±1	48.5±1.5
Elongation at break (%)	28.5±3	40±2	49.5±2
Toughness (MPa)	874	1370	1868.5
Scratch hardness (kg)	>10.0	>10.0	>10.0
Impact resistance (cm)	>100	>100	>100
Bending diameter (mm)	<1	<1	<1
Initial degradation temperature (°C)	284	288	290

Initial degradation temperatures of pristine hyperbranched epoxy and its nanocomposites were given in Table 9 and TGA curves were shown in Figure 17. From the results it was found that the initial degradation temperature of hyperbranched epoxy thermoset increased up to 23 °C after formation of nanocomposite with 1.5 wt% nanohybrid. The initial degradation temperature increased with the increase of amount of nanohybrid loading.

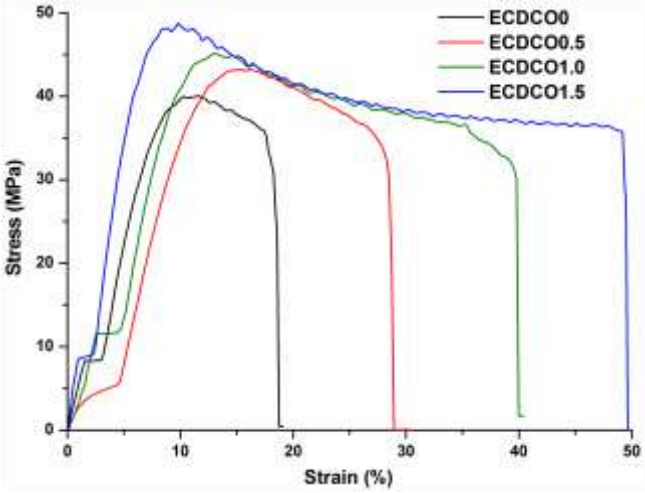

Figure 16 Stress-strain profiles for pristine thermoset and nanocomposites with carbon dot and carbon dot reduced Cu_2O nanohybrid

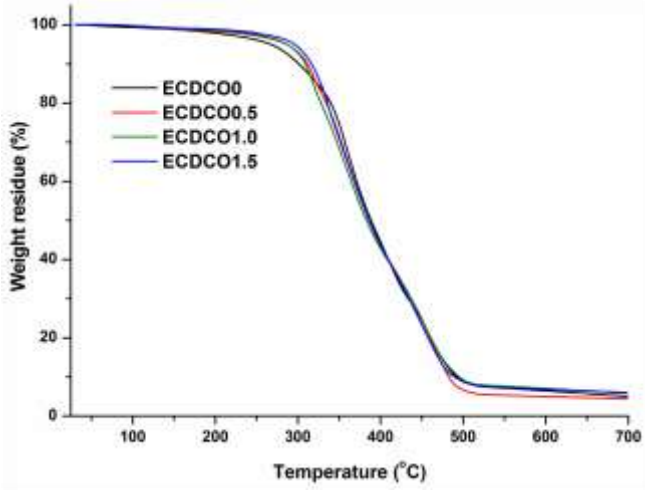

Figure 17 TGA curves for pristine thermoset and its nanocomposites with nanohybrid

The antibacterial study of the nanocomposites is shown in the Figure 18 in different bacterial species.

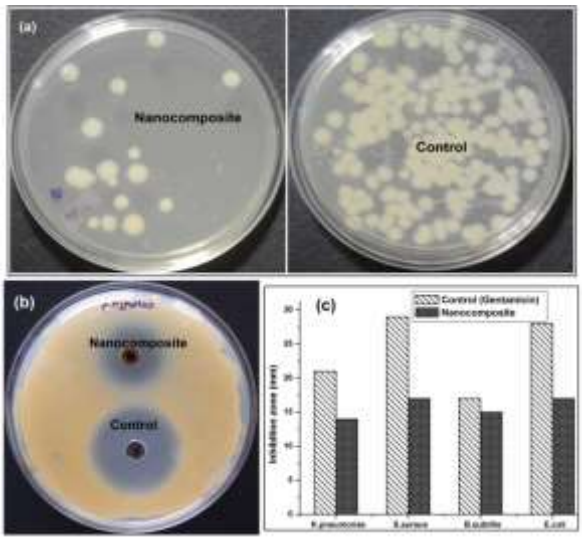

Figure 18 Antibacterial activity of carbon dot reduced Cu_2O nanohybrid/hyperbranched epoxy nanocomposites

OMMT-carbon dot reduced Cu_2O nanohybrid and its nanocomposites with hyperbranched epoxy

OMMT-carbon dot reduced Cu_2O nanohybrid was prepared by reduction of $Cu(OAC)_2$ solution using carbon dot in the presence of OMMT. The reduction was done by same procedure as like carbon dot reduced Cu_2O nanohybrid. However, here OMMT was used as a stabilizer as well as for high performance nanocomposites. The nanohybrid was coded as ECDCONC. The hyperbranched epoxy nanocomposite with 1, 2 and 3 wt% ECDCONC nanohybrid by solution technique were coded as ECDCONC1, ECDCONC2 and ECDCONC3 respectively. The formation of the nanohybrid was shown in Scheme 2. From TEM images of ECDCONC (Figure 19a and Figure 19b) it can be seen that the small tiny particles of carbon dot and Cu_2O are attached on the surface as well as inside the platelets of OMMT. Two types of lattice spacing of 0.27 and 0.36 nm were found in TEM image, which correspond to the d_{111} spacing of Cu_2O and d_{002} spacing of carbon dots, respectively as shown in Figure 19c. In the XRD pattern (Figure 20) of ECDCONC the same crystallographic spacing of carbon dot reduced Cu_2O nanohybrid were found along with d001 and d002 peaks at 2θ (°) = 7.08 and 19.82 respectively for OMMT crystal. However, in this case the intensity of Cu_2O peaks were very low due to the absorption of Cu_2O nanoparticles into the OMMT platelets as well as masking effect by OMMT as amount is higher than Cu_2O.

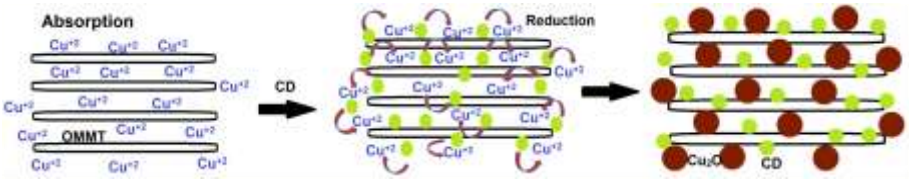

Scheme 2 Formation of ECDCONC

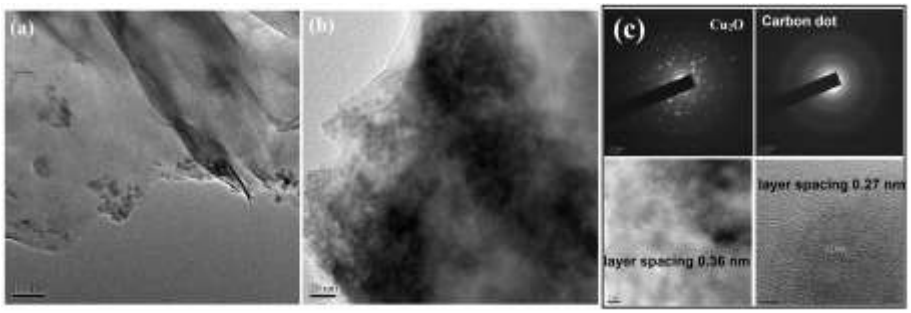

Figure 19 TEM images of ECDCONC at (a) 100 nm and (b) 20 nm resolutions; and (c) SAED patterns of Cu_2O, carbon dot and their interlayer spacings obtained from TEM images

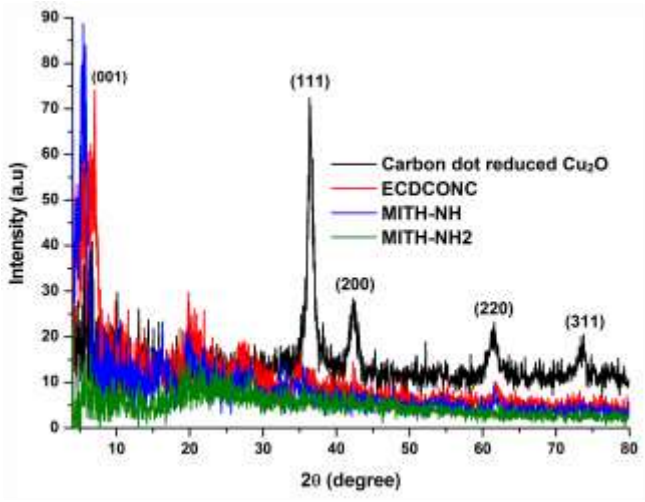

Figure 10 XRD patterns of the nanohybrids and MITH-NH2 nanocomposite

For objective 4: Immobilization of natural biocide such as neem oil, curcumin, *H. aromatica* oil, etc. for antifouling property by the nanoclay and nanohybids has been completed.

Preparation of neem oil immobilized OMMT

The hyperbranched epoxy/immobilized OMMT nanocomposites were prepared by solution technique. Three different amounts (1, 2.5 and 5 wt%, separately) of neem oil modified OMMT dispersed in THF were added to the hyperbranched epoxy and stirred magnetically for 5 h at room temperature followed by sonication for 10 min at 60% amplitude and 0.5 cycles with acoustic power density 460

W/cm^2. The 50 wt% (with respect to hyperbranched epoxy) poly(amido-amine) was mixed homogeneously with the above mixtures and coated on glass and steel plates. The plates were kept 24 h under vacuum at room temperature to remove THF and air bubbles. Finally, the plates were cured inside a furnace at 100 °C for specified time interval by optimizing the swelling values. The nanocomposites were coded as NONC1, NONC2.5 and NONC5 for 1, 2.5 and 5 wt% neem oil modified OMMT respectively. Similarly, hyperbranched epoxy nanocomposite with 2.5 wt% unmodified OMMT was prepared and coded as ONC2.5. The pristine hyperbranched epoxy thermoset was coded as NONC0.

Preparation of H. aromatica oil immobilized OMMT

In case of *H. aromatica* oil immobilized OMMT, 0.5 g of the hydrophilic bentonite clay was taken and swelled in 3 mL of ethyl acetate. The oil was dissolved in ethyl acetate and added to the clay dispersion. The dispersion was stirred at 40 °C for 24 h. The clay was then washed with ethyl acetate to remove the unused oil and kept for drying in an oven at 45 °C. Similarly, OMMT clay was modified with the oil. To determine the effect of the oil on the clay-polymer interaction, three systems were taken, viz. OMMT epoxy nanocomposite (HGEC), *H. aromatica* oil modified OMMT epoxy nanocomposite (HGEMC), *H. aromatica* oil modified bentonite clay epoxy nanocomposite (HGEB) and dendritic poly(amido-amine) modified bentonite clay (MNC). In each case 5 weight % (with respect to epoxy) of the un-modified/modified nanoclay was swelled in 5 mL of THF in a magnetic stirrer, followed by ultrasonication. The previous work from the same laboratory proved that 5 weight % nanoclay loading increases the mechanical properties of the nanocomposites to a significant extent. Swelled nanoclay was mixed with the prepared hyperbranched epoxy resin, with the help of a magnetic stirrer at 50 °C for 6 h. Further dispersion of the nano clay with the polymer matrix was assisted by 30 min of ultrasonication. Unmodified bentonite clay epoxy nanocomposite was also prepared which showed distinct phase separation on curing. Therefore, it was not considered for further studies.

Preparation of the silver-reduced graphene oxide (Ag-RGO) immobilized curcumin

Ag-RGO nanohybrid was prepared as according to our recently reported method. In brief, Hummer's method was employed to produce graphene oxide (GO) from graphite. GO (500 mg) was dispersed in 100 mL of water using ultrasonication for about 20 min. Then, *Colocasia esculenta* leaf extract was added into the above dispersion and stirred. 0.03 M $AgNO_3$ solution was added to the mixture and again stirred for 8 h. Ag-RGO settled down after the completion of the reaction. This was washed successively by centrifugation and kept for drying. Ag-RGO (0.5 g) was dispersed in 15 mL THF by sonicating it for 15 min. 0.25 g of curcumin was dissolved separately in 5 mL of THF and added to the above dispersion. The dispersion was stirred at room temperature for 4 h, followed by 30 min of ultrasonication. It was centrifuged for 15 min at 1006×g (3000 rpm) and the supernatant (in THF) was discarded. The process was repeated in order to remove undesired components. The immobilized system (Ag-RGO-Cur) was collected and allowed to dry at room temperature.

Preparation of the epoxy/ Ag-RGO-Cur nanocomposites

Ag-RGO-Cur was dispersed in THF and incorporated into the hyperbranched epoxy resin in 1, 2 and 3 wt%, separately. The mixture was stirred at 50 °C for 4 h. Then, it was ultrasonicated for 15 min in each case. The prepared nanocomposites were coded as HGGS1, HGGS2 and HGGS3 according to the content (wt%) of Ag-RGO-Cur present in them.

Preparation of MWCNT-CuO nanohybrid immobilized nystatin

MWCNT (0.5 g) was dispersed in water using ultrasonication for 45 min. Trition X-100 (0.15 g, 30 wt% of MWCNT) was added into the dispersion and stirred at 60 °C for 3 h. CuO nanoparticles were prepared *in situ* by following our recently reported protocol with slight modification. Briefly, 1.42 g of copper acetate was dissolved in the aforementioned dispersion using a magnetic stirrer. The amount was taken at 1:2 ratio of MWCNT to CuO. Then, 1 mL of *Terminalia chebula* fruit extract (aqueous) was added to the reaction mixture and stirred for another 2 h at room temperature. The mixture was sonicated for 30 min (amplitude: 60% and cycles: 0.5). Then, the suspension was centrifuged for 10 min at 1006×g (3000 rpm). This was repeated several times to remove unwanted components. Finally the residue was washed with tetrahydrofuran (THF, SD fine Chem., India) for 2-3 times and allowed to dry at room temperature to obtain the desired nanohybrid (CNT-CuO).

CNT-CuO was then dispersed in THF by sonication for 10 min. 0.5 g of nystain was added to the dispersion and stirred at room temperature for 3 h, followed by ultrasonication for 15 min. This antibiotic immobilized system (CNT-CuO-Nys) was again centrifuged at 1006×g (3000 rpm) for 15 min. The residue was collected and dried at room temperature. This was used as the antibiotic immobilized nanohybrid for the preparation of nanocomposites.

Preparation of 2-Methyl-4-isothiazolin-3-one hydrochloride (MITH) immobilized ECDCONC

2-Methyl-4-isothiazolin-3-one hydrochloride (MITH) was immobilized on ECDCONC by combined effect of mechanical shearing and ultrasonic forces at room temperature. In a typical process, 0.5 g ECDCONC was dispersed in 25 mL THF under constant stirring for 30 min in a 60 mL glass bottle. An amount of 20 wt% of MITH (0.1 g) with respect to ECDCONC nanohybrid was added to it and stirred continuously for 2 h at room temperature followed by ultrasonication for 10 min. MITH immobilized nanohybrid was coded as MITH-NH. The hyperbranched epoxy nanocomposites with 1, 2 and 3 wt% of MITH-NH by solution technique were coded as MITH-NH1, MITH-NH2 and MITH-NH3 respectively.

Preparation of nanocomposites

Three nanocomposites were prepared by incorporating 1, 2 and 3 wt% of CNT-CuO-Nys to 5 g of hyperbranched epoxy resin in each case, separately. Then the mixed system was allowed to stir for 5 h at 50 °C and sonicated for 15 min. The nanocomposites were encoded as HGCC1, HGCC2 and HGCC3 according to the weight percentages of CNT-CuO-Nys.

For objective 5: Characterization of the prepared nanohybrid immobilized biocide systems by different analytical and instrumental techniques has been completed.

Characterization of neem oil immobilized OMMT and its nanocomposites

The neem oil immbolized OMMT (NO-OMMT) and its nanocomposites were first characterized by FTIR study (Figure 21). The characteristic bands are given in Table 10.

Table 10: FTIR bands

Bands	Position in OMMT (cm^{-1})	Position in Neem oil (cm^{-1})	Position in NO-OMMT (cm^{-1})	Position in NONC2.5 (cm^{-1})
-NH	3640	-	3627	-
-OH	3414	3472	3427	3400
-CH	2928	2928	2928	2928
C=O (ester)	-	1750	1736	-
C=O (amide)	-	-	1627	1640
C-O	-	1458	1471	1458
Si-O	1037	-	1037	1037
Al-O-Si	527	-	527	565
Si-O-Si	462	-	462	462

The presence of ester bands at 1736 (C=O) and 1471 (C-O) cm^{-1} in NO-OMMT supports the immobilization is done successfully.

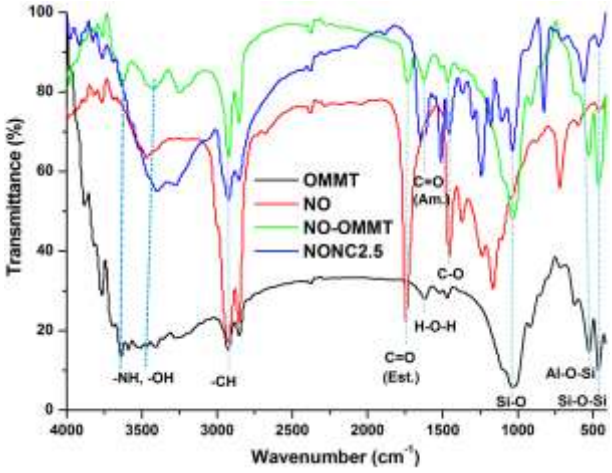

Figure 21 FTIR spectra

The immobilization of neem oil into OMMT was again confirmed by XRD study (Figure 22). The d_{001} spacing for OMMT at $2\theta = 4.2°$ was shifted to 2.7° in NO-OMMT which reveals that the long chain fatty acid of neem oil is intercalated into the clay galleries. In case of nanocomposite this peak

was completely diminished which indicates the hyperbranched epoxy chains are exfoliated the clay platelets.

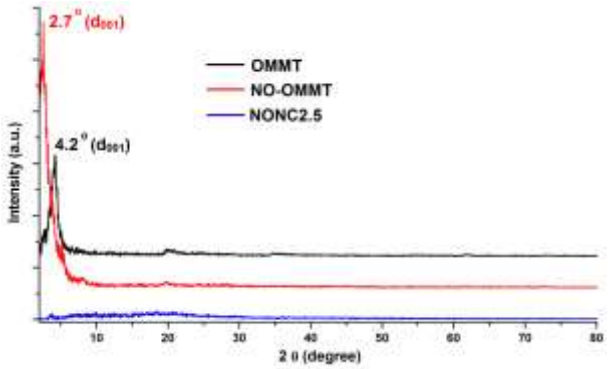

Figure 22 XRD patterns

The TEM image discloses the actual picture of state of dispersion of clay in the nanocomposites. Figure 23 reveals the homogenous dispersion of disordered structure of clay layers in the epoxy matrix. The image shows both the exfoliation and intercalation of clay layers in hyperbranched epoxy matrix. SEM is also a valuable technique for examining the morphology of the nanocomposites. Uniform dispersion of clay in the hyperbranched epoxy was also confirmed by the SEM image of the fracture surface of the nanocomposite (Figure 24). This uniform dispersion is due to the strong physico-chemical interactions of neem oil immobilized clay with hyperbranched epoxy and the hardener.

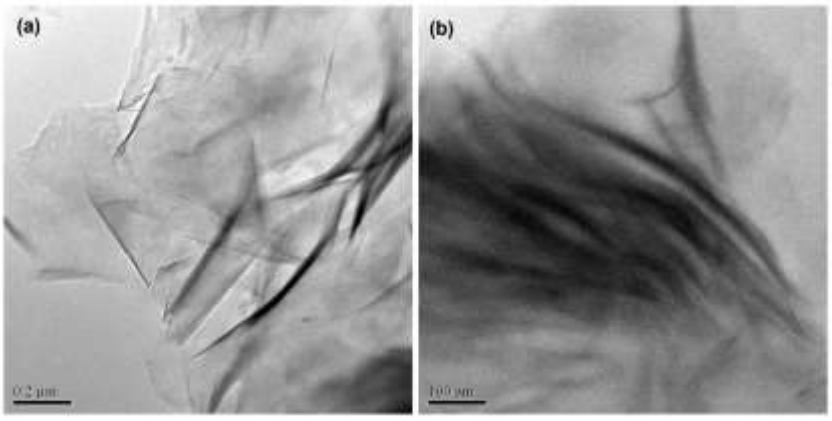

Figure 23 TEM images of NONC2.5 at (a) 200 and (b) 100 nm magnifications

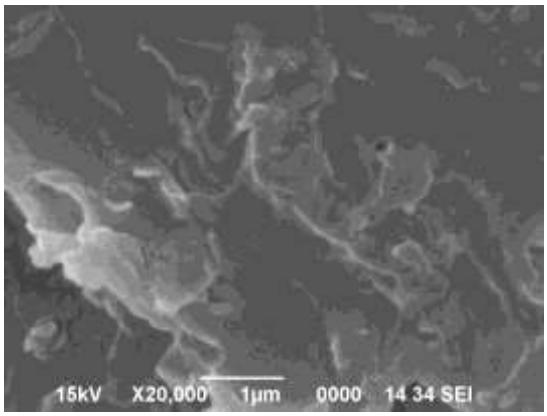

Figure 24 SEM image of NONC2.5

Characterization of H. aromatica oil immobilized OMMT

XRD pattern (Figure 25a) showed the peak shifting (2θ value) from 6.75° (OMMT) to 4.11° (modified OMMT) as shown in Figure 3a. This corresponds to the increase in the basal spacing from 1.31 nm to 2.11 nm, which ascertains the delamination of the clay layers upon interaction with the oil. The nanocomposites exhibited a kind of exfoliating behavior, as the peak was diminished to a considerable extent. This ascertains that the oil-modified OMMT clay has very good interaction with the polymer matrix.

X-ray diffraction patterns of the bentonite clay, modified bentonite clay and the hyperbraned epoxy clay nanocomposites are shown in Figure 25b. For pristine bentonite clay, the basal spacing is 1.29 nm, as calculated from the peak position (2θ= 6.82°) in the diffractogram using the Bragg's equation. The *H. aromatica* oil modified bentonite clay showed an increase in the basal spacing (*d*= 1.45 nm), which corresponds to the peak at 2θ= 6.09°. This confirms the intercalation of the clay layers as a result of modification. Furthermore, this imparts organophilic behavior to the nanoclay. The *d*-spacing of the clay layers in the nanocomposite is found to be 2.81 nm. This delamination demonstrated the insertion of the hyperbranched epoxy chains in the basal spacing of the modified clay and formed an intercalated nanocomposite.

Furthermore, the intercalation of the chains between the clay layers was evident from the TEM micrographs (Figure 26). The interlayer spacing of the clay layers in the HGEB was found to be increased (2.75 nm) from the pristine nanoclay (1.32 nm) (Figure 26a and b), which is very close to the value measured through the XRD pattern (2.81 nm). In case of other nanocomposites, the TEM images showed exfoliation of the clay layers, which was in agreement with the XRD patterns (Figure 26c and d). HGEMC showed partially exfoliated clay layers, which ascertains strong interaction of the nanomaterials with the polymer matrix.

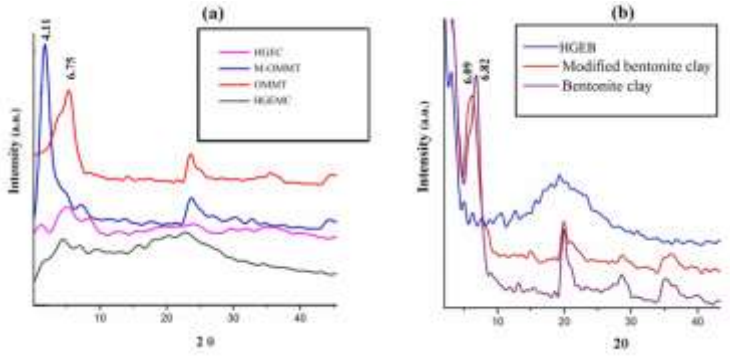

Figure 25 XRD patterns of (a) nanocomposites and (b) nanomaterials

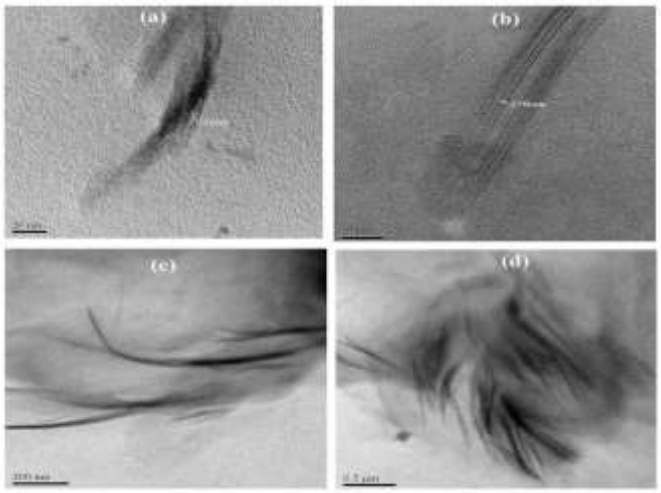

Figure 26 TEM images of (a) & (b) nanoclay and (c) & (d) nanocomposites

Characterization of the clay, silver-clay and Ag-RGO-Cur nanocomposites

TEM micrographs (Figure 27) show uniform distribution of silver nanoparticles embedded in clay layers. Partially exfoliated clay layers prevented the agglomeration of the nanoparticles by embedding them within the layers.

UV-visible spectroscopy (Figure 28) showed the formation of Ag-RGO, with peaks at 407 and 330 nm for AgNP and RGO. The second peak is due to the n-π* electronic transitions of the aromatic carbon bonds of RGO. Curcumin showed its characteristic absorbance peak at 417 nm, which was observed to be broadened upon immobilization onto Ag-RGO. This clearly indicates the interaction of curcumin with the nanohybrid. Similar observations were witnessed for the nanocomposites. Presence of the above mentioned peaks in the HGGS proves the presence of Ag-RGO-Cur inside the hyperbranched epoxy matrix.

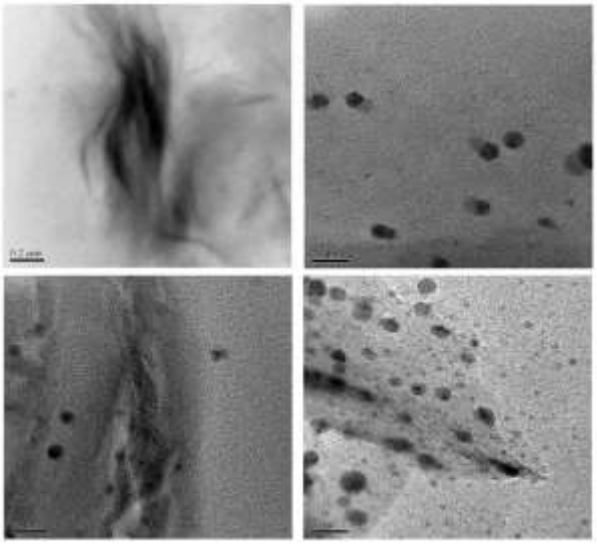

Figure 27 TEM images of clay/silver nanocomposite

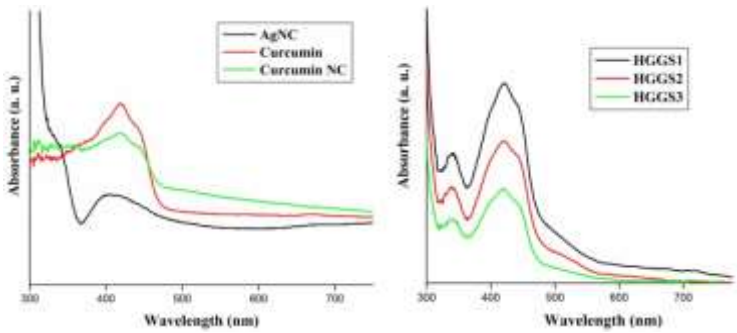

Figure 28 UV-visible spectra of Ag-RGO nanocomposites

TEM micrographs of the nanocomposites are presented in Figure 29. Narrow size distribution of AgNP was clearly visible from the histogram, where maximum particles lie between of 10-15 nm. Moreover these particles are embedded within the RGO sheets. Again, Ag-RGO was distributed in the hyperbranched epoxy matrix. An RGO sheet with lattice fringe spacing 0.68 nm was observed over AgNP. This indicated that the nanomaterials have efficient interaction between them and the nanohybrid is strongly interacting with the epoxy matrix. The π-π electron affinity plays the vital role in this case. These types of interaction lead to the enhancement of mechanical attributes in a nanocomposite system.

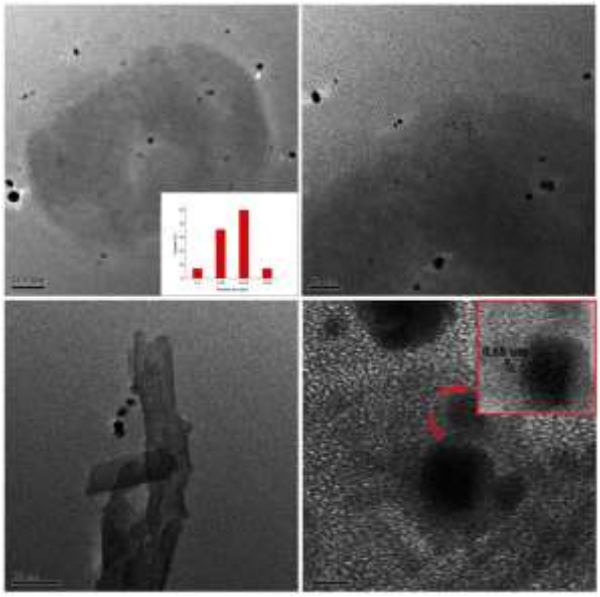

Figure 29 TEM images of Ag-RGO nanocomposites

Characterization of MWCNT-CuO nanohybrid immobilized nystatin

UV-visible spectroscopy is a strong tool to detect the generation of metal nanoparticles. MWCNT did not show any peak in the UV-visible region, due to their poor stability in the aqueous medium (Figure 30). In the figure, it is clearly visible that the characteristic plasmon peaks of CuO were present in case of CNT-CuO at 232 and 325 nm. Again, CNT-CuO-Nys showed a subtle blue shift of the former peak to 227 nm, along with the multiple peaks of nystatin at 289, 303 and 318 nm. Similar spectral behavior was evidenced for the nanocomposite. This indicates the presence of CNT-CuO-Nys in the nanocomposite.

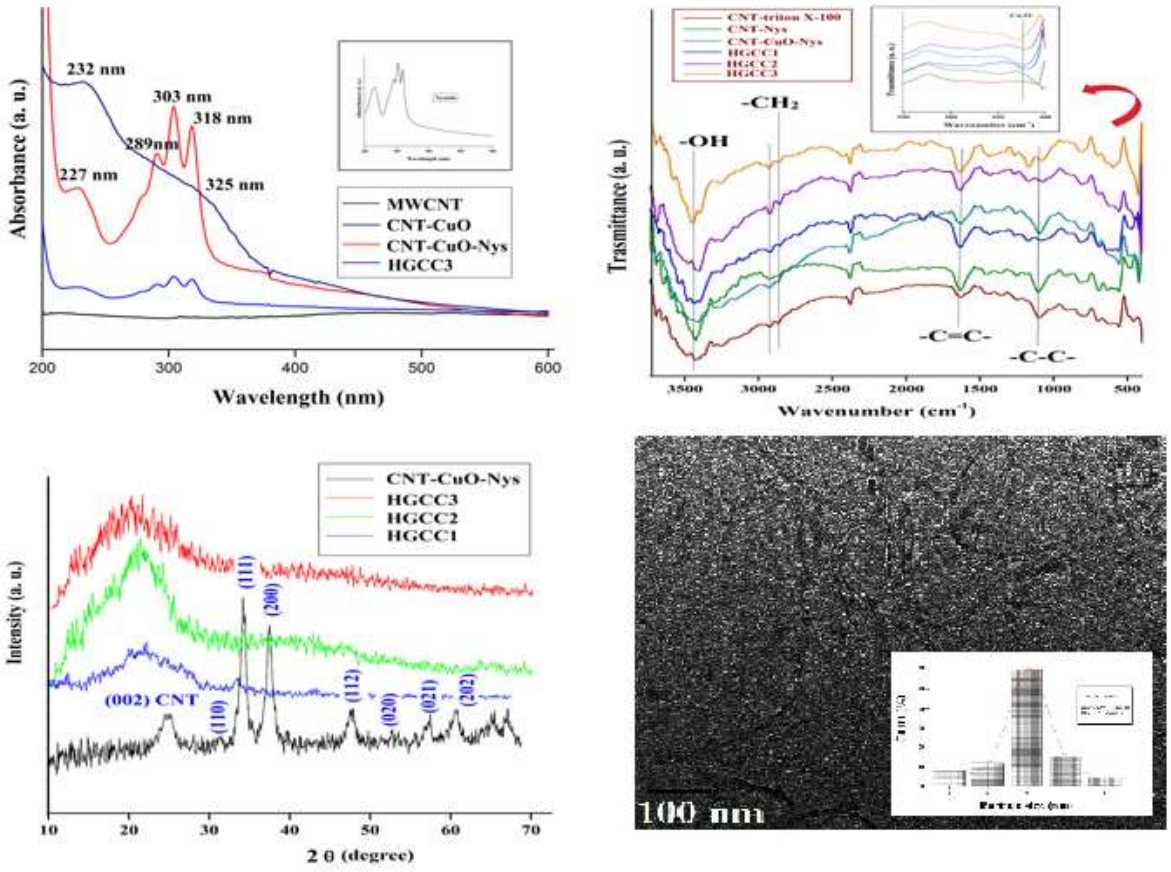

Figure 30 UV-visible spectra of MWCNT, CNT-CuO, CNT-CuO-Nys, HGCC3; FTIR spectra of modified CNT, CNT-CuO, CNT-CuO-Nys and the nanocomposite thermosets; XRD patterns of CNT-CuO-Nys and the nanocomposites and TEM micrographs of the nanocomposite

FTIR spectra were recorded and presented in Figure 30. Triton X-100 modified MWCNT showed the presence of characteristic bands of poly(ethylene glycol) at 3422 (-OH stretching) and 1137 cm^{-1} (C-C stretching). These bands were evidenced for all the samples. Presence of C=C bonds of MWCNT is shown by band at around 1653 cm^{-1}. This band sharpened in case of nanohybrid and nanocomposites, which may be due to the combined effect of nystatin and MWCNT. Other characteristic bands of nystatin were evidenced at 2880 and 2943 cm^{-1}, due to the symmetric and asymmetric vibrations of -CH_2 groups. Bands at around 427-421 cm^{-1} were observed for Cu-O linkages (onset). These bands are clearly visible in case of the nanocomposite thermosets. The bands for epoxy ring are generally observed at around 915–839 cm^{-1}. Absence of the bands ascertains the successful curing of nanocomposite.

XRD patterns of the nanocomposites are shown in Figure 30. CNT-CuO-Nys showed a peak at 2θ value 24.7°, due to the presence of graphitic structure of MWCNT. The pattern showed distinct peaks at around 31.23 , 34.16, 37.52, 47.81, 53.38, 57.54 and 60.43° correspond to the monoclinic structure of CuO, with Bragg's reflection planes {110}, (111}, {200}, {112}, {020}, {021} and {202} (JCPDS

card No. 80-1917). These peaks were not distinctly visible in case of nanocomposites may be due to masking effect. This is attributed to efficient interaction of the nanohybrid with hyperbranched epoxy matrix. However, small amount of nanomaterials and their embedded structure within the epoxy matrix directly influence their XRD patterns. A broad peak was observed at around 2θ=23°, which stands for the amorphous nature of hyperbranched epoxy system.

TEM micrograph shows the presence of 16 layers of the dispersed MWCNT in the nanocomposite. The external and internal diameters of the tubes were 18 and 4.9 nm respectively (Figure 30). Elongated sphere shaped CuO nanoparticles (with width 6.7 nm) were residing inside the walls of the tube. Also spherical particles (with diameter 7.1 nm) were visible within the tubes. This suggests that particles with different shapes were present in the nanocomposite. Nanoparticles, thus were found to be residing 'in and on' the nanotubes. The overall distribution is shown in Figure 30 (c, d) where it is clear that the nanohybrid is uniformly located within the hyperbranched epoxy matrix. The π-π electronic interaction of nanotubes with triton X-100 and nystatin helps in proper stability of the CNT-CuO-Nys system. Further, hyperbranched epoxy matrix stabilized the nanohybrid sterically as well as via π-π stacking. These interactions aid to the mechanical properties of the nanocomposites.

Characterization of 2-Methyl-4-isothiazolin-3-one hydrochloride (MITH) immobilized ECDCONC

After immobilization of MITH the d_{001} crystallographic peak of OMMT was shifted from 2θ (°) = 7.08 to 5.45. Thus the interlayer spacing of OMMT increases from 1.2 to 1.6 nm after immobilization of MITH. As a result, d_{001} peak in XRD analysis (2θ = 5.45°) was completely vanished after formation of nanocomposite as found in Figure 20. The direct visualization of well dispersed OMMT platelets as well as carbon dot reduced Cu_2O nanohybrid particles were found in TEM images (Figure 31) of nanocomposite. The well dispersed and disordered arrangement of clay layers inside the hyperbranched epoxy matrix was found in Figure 31a and 31c. The dispersion of the OMMT platelets and the carbon dot reduced Cu_2O nanohybrid particles are shown in Figure 31b, where the carbon dot reduced Cu_2O nanohybrid particles are attached with the OMMT surface and well-separated from each other without aggregation. In Figure 31d the intercalation behavior of OMMT platelets by the matrix was found. The interlayer spacing between the OMMT platelets was found to be ~1.3 nm as shown in Figure 31d. This is because of the hyperbranched epoxy chains intercalate the clay galleries by the strong interactions with the OMMT platelets assisted by immobilized MITH.

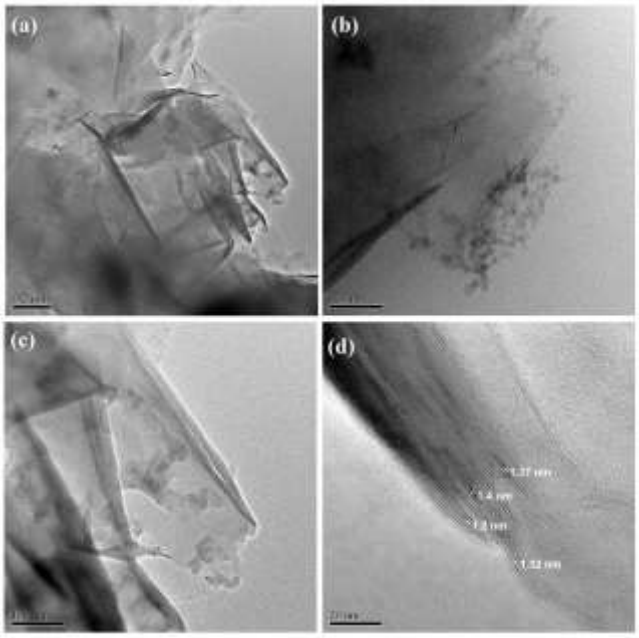

Figure 31 TEM images of MITH-NH2 at different resolutions and positions: (a) at 0.2 μm, (b) 100 nm, (c) 100 nm at different position and (d) OMMT layer spacing at 20 nm resolution

For objective 6: Performance study of the nanohybrid immobilized biocide nanocomposites as marine-coating materials is done. Some preliminary investigations are performed in this regard. The details including field study will be performed by help of the NRB collaborator.

Performance of the neem oil immobilized OMMT nanocomposites

The tensile strength, elongation at break, scratch hardness, impact resistance and bending of the nanocomposites are given in Table 11.

Table 11 Performance of pristine hyperbranched epoxy and its nanocomposites with neem oil immobilized OMMT

Parameter	NONC0	ONC2.5	NONC1	NONC2.5	NONC5
Swelling value (%)	24±1.0	21±0.4	22±0.8	24±0.2	29±0.6
Tensile strength (MPa)	40±1	57±1	48±4	62±3	56±2
Elongation at break (%)	18.5±0.5	19±1.5	43±2	56±5	69±4
Toughness (MPa)[a]	540	834	1637	2994	2680
Scratch hardness (kg)[b]	9.0±0.5	10.0	>10.0	>10.0	>10.0
Impact resistance (cm)[c]	>100	>100	>100	>100	>100
Bending diameter (mm)[d]	<1	<1	<1	<1	<1
Initial degradation temperature (°C)	267	282	278	285	288

For the antimicrobial activity, the nanocomposites were tested with different gram(+) bacteria like *Bacillus subtilis* and *Staphylococcus aureus*; and gram(-) bacteria like *Klebsiella pneumonia*, and *Pseudomonas diminuta*. The antibacterial test is shown in Figure 32 at different dose level of neem oil immobilized OMMT in nanocomposite.

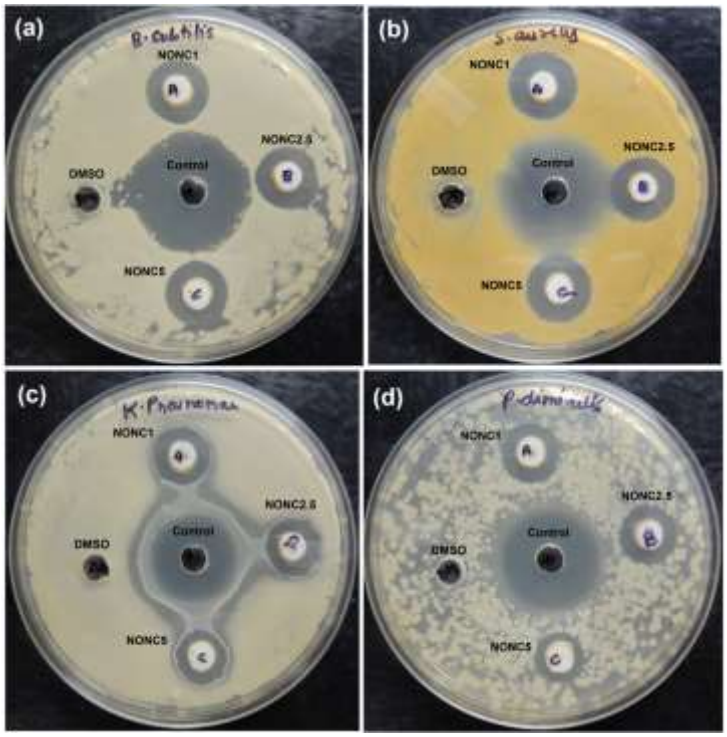

Figure 32 Antibacterial study; zone of inhibition of DMSO (100%), NONC1, NONC2.5, NONC5 in (a-c) different gram(+) and (-) bacteria

Performance of the H. aromatica oil immobilized OMMT nanocomposites

The mechanical properties were analyzed by determining the tensile strength, elongation at break, impact resistance, scratch hardness and bending values of the three nanocomposite thermosets (Table 12).

Table 12 Performance of clay/epoxy nanocomposites

Property	HGE	HGEB	HGEC	HGEMC
Tensile strength (MPa)	38-40	48-50	50-52	56-59
Elongation at break (%)	20-22	15-17	14-16	11-13
Impact resistance (m)	>1	>1	>1	>1
Scratch hardness (kg)	>10	>10	>10	>10
Bending (mm)	<1	<1	<1	<1
Adhesive strength (MPa) (wood)	>770	>1640	>2620	>3680

The zone of inhibition for each microorganism was tested taking the material concentration at their MIC values. Here also M-OMMT, HGEB and HGEMC exhibited good activity against the bacterial species (Figure 33). This indicated that the oil modified OMMT-clay imparted the activity to the nanocomposites. However, the effect was different for different microbes. HGEMC exhibited excellent biocompatibility as well as best material properties amongst the prepared nanocomposites. Therefore, HGEMC was only considered for the further studies.

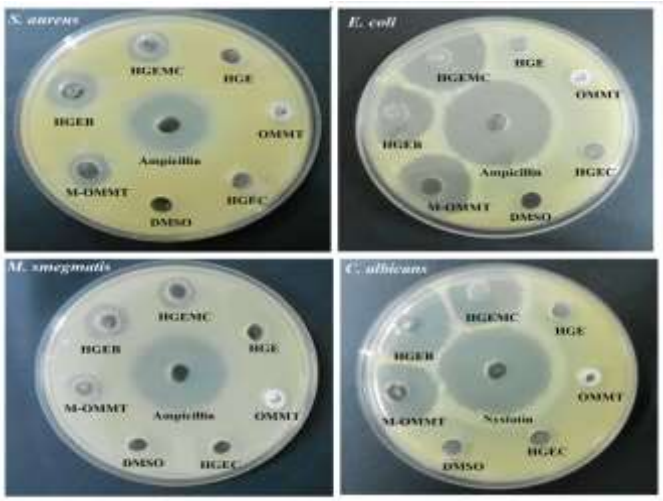

Figure 33 Antimicrobial assay

Performance of the clay, silver-clay and Ag-RGO-Cur nanocomposites

MIC was calculated for the nanocomposites against *S. aureus* and *C. albicans* (Figure 34). Our previous report demonstrated enhanced inhibitory effect of Ag-RGO over the individual components. Further, immobilization of curcumin shows more effective increment, which can be clearly estimated by analyzing the resultant MIC values. Immobilization of biomolecules onto the nanomaterial surface increases its efficacy by synergistic effect at bio-nano-interface. Antimicrobial activity of a material depends on its surface structure. Ag-RGO provides a high surface area, which complemented the activity of curcumin. However, in case of the nanocomposites, lower MIC values were observed, which can be attributed to the indirect exposure of the active components to the microbes. Additionally, the significant reduction of the nanohybrid with respect to the matrix is also responsible for the above findings. However, it is expected that the active components may be leached out with due course of time and antifouling action will be sustained.

Again, Figure 35 indicates clear decrement of the microbial growth with time when incubated with the nanocomposite (HGGS3). Absorbance of *S. aureus* shows exponential growth with time in case of control. On the other hand, their growth decreases and come to a steady state in presence of the nanocomposite. This ascertains that the nanocomposite possesses antibacterial properties. Similar absorbance profile was witnessed for *C. albicans* in presence of the nanocomposite film. The active component may leach out very slowly which could interact with the microorganisms and cause

damage to their cellular organization. Further, adherence of microbes to the nanocomposite surface causes microbial cell lysis, which leads to a decrease in their population and stops them for further growth. This type of activity is essential for an antimicrobial material, which could prevent infection at surgical sites, by following the aforementioned mechanism (Figure 36).

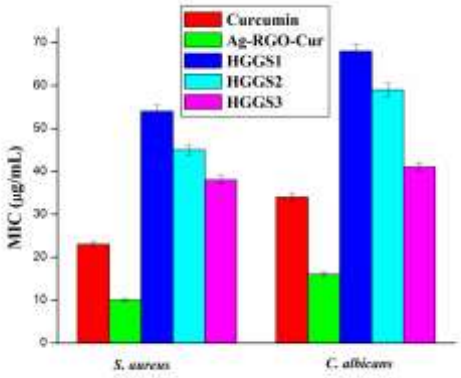

Figure 34 MIC of the nanocomposites against bacteria and fungi

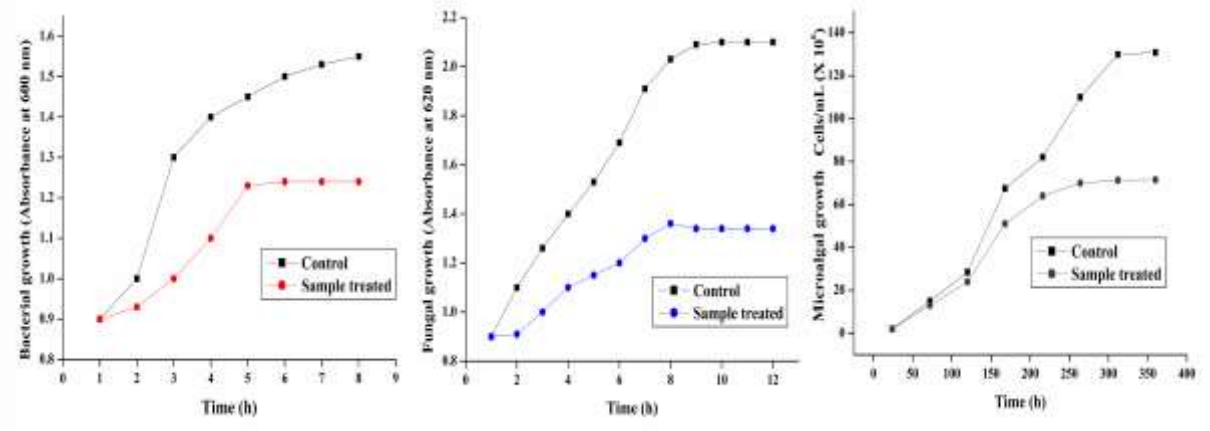

Figure 35 Inhibition of growth of (a) Bacteria, (b) Fungus and (c) Microalga in presence of the nanocomposite

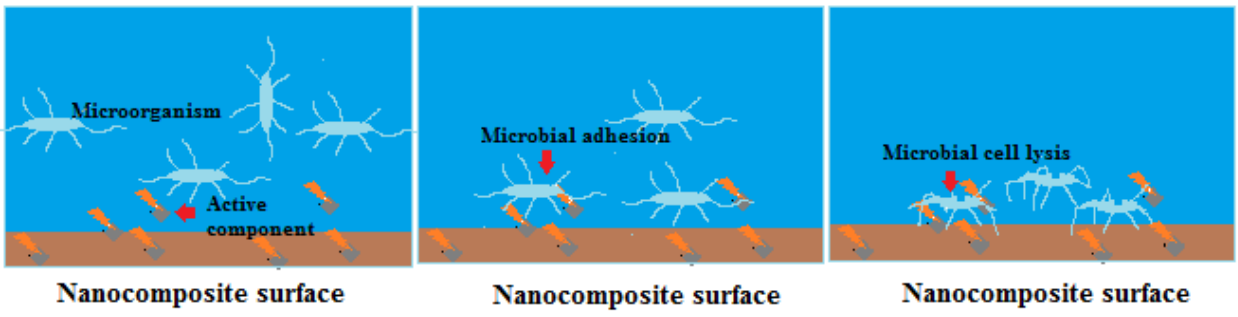

Figure 36 Probable mechanism of the antifouling activity of the nanocomposite

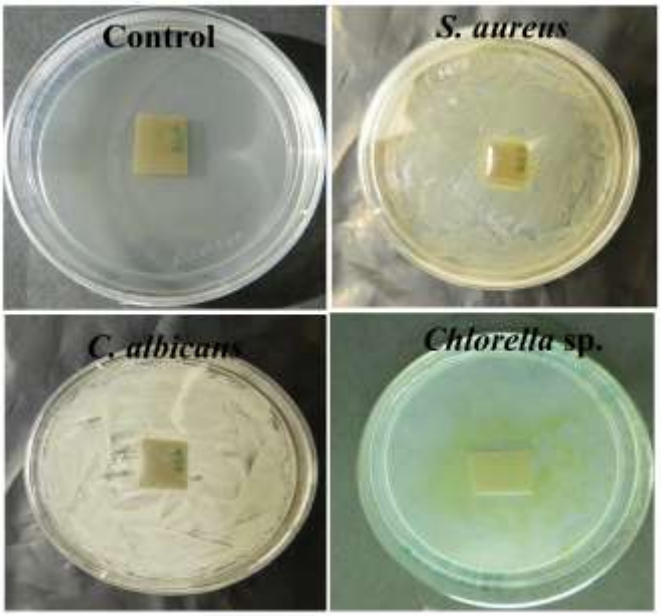

Figure 37 Antifouling activity of the nanocomposites in the proximities of bacteria, fungi and microalgae

Unlike bacteria and fungi, the growth of microalgae was not monitored spectrophometrically. The microalgal growth was monitored by measuring the cell concentration in a Neubauer haemocytometer (in triplicates) at regular intervals of 48 h for 15 days. From Figure 35, a gradual progressive decline in microalgal growth is evident. This may be attributed to the fact that the microalgae could not adhere to the nanocomposite surface and deposited at the bottom of the test tubes, whereby demonstrating competitive growth inhibition. Additionally, the light absorbing capacity of RGO may also help in prevention of microalgal growth. Hence, the present nanocomposite has the potential to provide a surface that could prevent microalgal growth upon its surface. Marine coatings with such properties may help in resisting the growth of different fouling microalgae.

Moreover, assays were carried out to examine the possibility of microbial growth in the proximity of the nanocomposite. Figure 37 shows clear evidence that neither the bacteria nor the fungi could grow on the surface of the nanocomposite. On the other hand, their uniform growth is visible throughout the rest parts of the plates. Although the microalgal growth is not uniform, no growth is seen on the surface of the nanocomposite.

Thus, the aforesaid assays confirmed that the nanocomposite could prevent the growth of the two most notorious microorganisms responsible for causing infection at surgical sites. This may be utilized to design protective coatings for surgical implants and devices. Moreover, the surface was able to inhibit microalgal fouling over it, which may endorse the same material for utilization in advanced marine coatings. However, in both the cases, toxicity of the materials should be analyzed properly.

Performance of MWCNT-CuO nanohybrid immobilized nystatin

Tensile strength was augmented to a significant extent upon formation of the nanocomposites from the pristine system (38 MPa). This increment was directly proportional to the loading of CNT-CuO-Nys into the epoxy matrix. In this case MWCNT plays the lead role. It is well known to the scientific community that incorporation of MWCNT abets to the mechanical strength of a polymer. However, elongation and flexibility gets decreased. In the present case, use of Triton X-100, helps in maintaining the elongation and flexibility, due to its long flexible chain structure. Further, nystatin also aids to the augmentation of this property. Therefore, it was witnessed that both tensile strength and elongation at break increased from the pristine matrix on loading of 1 and 2 wt% CNT-CuO-Nys in the nanocomposites. However, on 3 wt% loading though the tensile strength increased, a slight decrement of the elongation value was observed. Competition between restriction of molecular mobility and plasticization affects this phenomenon, where the former overcomes the latter. Loading above this value showed phase separation at the time of curing. Thus, HGCC3 could be considered the best performing nanocomposite, in regard of overall mechanical properties. Moreover, the thermosetting nanocomposite could be folded to 180° curvature without damage. The variations of scratch hardness and impact resistance values were not possible to detect due to the limits of the instruments (Instrumental limits: scratch hardness = 10 kg and impact resistance = 1 m).

Lap sheer tensile adhesive strength of the nanocomposites was also increased to many folds than the pristine epoxy thermoset. Polar functionalities of triton X-100, nystatin as well as of hyperbranched epoxy help in augmentation of the adhesive strength. With increase in loading of CNT-CuO-Nys, these functionalities increase. Thus, they cause extensive interaction with the polar groups of wood substrate by secondary forces. Performance of nanocomposites reflects their potential as an excellent material for thin film applications. Further, focusing at the targeted field of application, their microbial fouling preventing capability and biocompatibility are to be monitored carefully.

MIC values of the nanomaterials and the nanocomposites are presented in Figure 38. Inhibitory effect of MWCNT was increased upon formation of CNT-CuO. Copper oxide and copper are used in a number of commercial products as antimicrobial agents, which prevent the growth of a broad spectrum of microbes. Thus, the increment is obvious in case of CNT-CuO. Immobilization of nystatin further enhanced this efficacy. However, activity of the material was found to be strong against *C. albicans*.

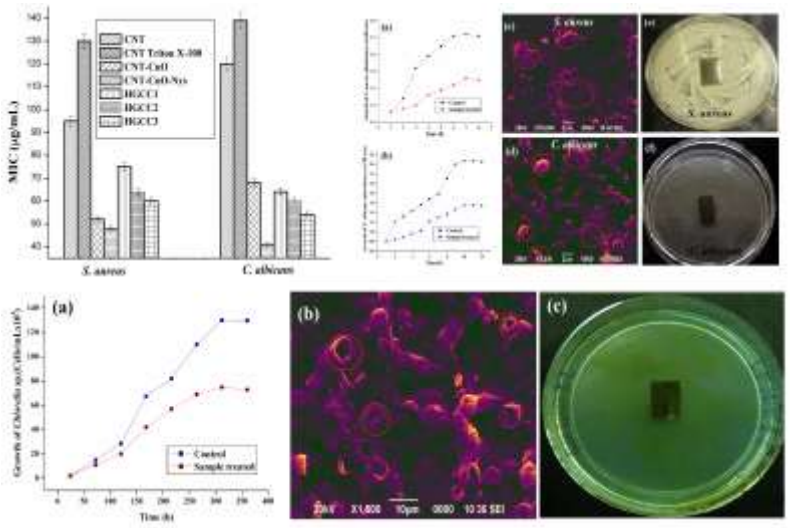

Figure 38 MIC against *S. aureus* and *C. albicans*; Inhibition of growth of (a) *S. aureus*, (b) *C. albicans*; SEM images of cell morphology alteration of HGCC3 adhered (C) *S. aureus*, (d) *C. albicans* and growth of (e) *S. aureus* and (f) *C. albicans* in the close vicinity of HGCC3 and (a) Growth inhibition of *Chlorella* sp. in presence of HGCC3, (b) SEM micrographs of microalgal cells, adhered on HGCC3 surface and (c) growth of the microalga in the proximity of HGCC3.

Nanocomposites showed inhibitory effect within the concentration range of 75-54 µg/mL. HGCC3 showed the lowest MIC value amongst the studied nanocomposites, which is owing to the amount of CNT-CuO-Nys within the matrix. Higher MIC values for the nanocomposites are attributed to the reduction in the amount of CNT-CuO-Nys as compared to that of hyperbranched epoxy. Further, microbial growth with time was monitored in presence of the nanocomposite (HGCC3). Both *S. aureus* and *C. albicans* grew in exponential manner in the control. Contrarily, in presence of HGCC3, their growth was hindered and a clear decrement in the absorbance was witnessed (Figure 38 a, b). Slow release of the active components may be responsible for this decrement. Reported literature suggests that adherence of microorganisms to such surfaces cause cell lysis, which restricts their proliferation upon it. Here also SEM micrographs show alteration of cell membranes in case of *S. aureus* and C. *albicans* (Fig. 28 c, d). In the figure, red marked portions clearly indicate that fragmentation, disruption and morphology alteration of microbial cells occured while they were adhered to HGCC3 surface. Thus, their growth was inhibited in presence of HGCC3. This assay confirms that both bacterial and fungal growths are hampered in presence of the nanocomposite. Materials with this kind of activity may be useful in the biomedical domain to design antimicrobial surface over implants and devices. Interestingly, the nanocomposite inhibited the growth of *S. aureus* and *C. albicans*, that cause most of the severe infections at surgical sites.

Figure 38 (e, f) clearly indicates the absence of bacterial or fungal growth in the close vicinity of HGCC3 surfaces, though their growth was observed throughout the plate. This again affirms the

aforesaid observation that the HGCC3 surface could prevent both bacterial and fungal growth. Leaching out of the active components from the matrix may prevent the microorganisms to come closer to the HGCC3 surface, which could be effective to avoid microbial fouling.

Figure 38 shows the growth curve of *Chlorella* sp (both control and treated) in BBM culture media. As evident from the growth curve, a decrement in growth was observed for the treated sample. At the end of the 13th day maximum cell density of 129.9×10^5 cells/mL was achieved in case of control which corresponds to a growth rate of 0.215 per day. The maximum cell density for the treated sample was 74.8 ×10^5 cells/mL at the end of the 13th day which corresponds to a growth rate of 0.191 per day. SEM micrographs showed shrinkage of the microalgal cells when they were adhered to HGCC3 surface (Fig. 38b). Complete disintegration of the nuclei is clearly visible from the figure (red marked). Thus, this confirmed that HGCC3 could prevent the proliferation *Chlorella* sp on its surface, which may be highly useful in the marine industry to prevent microalgal biofouling.

From Fig. 38 c microalgal adherence was not seen in the edges of the film and no microalgal growth was evident in close proximity of the film. These observations reveal that the nanocomposite film possessed inhibitory activity that prevents the growth of microalgae in its vicinity.

The overall antimicrobial assay ascertained that HGCC3 could prevent bacterial, fungal and microalgal fouling. This activity combined endorses the material for multifaceted advanced applications in the domains of marine and biomedical science.

Performance of MITH-NH nanocomposites

The percentage of swelling values of the cured nanocomposites and the pristine thermoset are given in Table 13. The swelling values of the nanocomposites decrease with the increase of amount of nanohybrid loading and thus the extent of crosslinking is increased. The values of mechanical properties for the nanocomposites and the pristine thermoset are given in Table 13. Tensile strength, elongation at break and toughness values of the pristine hyperbranched epoxy thermoset sharply increased after formation of nanocomposites with MITH-NH. The tensile strength of pristine thermoset increased from 40 to 72.5 MPa after formation of MITH-NH3. From the stress-strain profiles (Figure 39) it is found that elongation at break and toughness (area under stress-strain curve) of pristine thermoset were dramatically improved after formation of nanocomposites with MITH-NH. A 3 fold increment in elongation at break and 4 fold increment in toughness of the pristine system were observed for MITH-NH3. The improvements in scratch hardness and impact resistance could not be measured as the values for the nanocomposites have reached the highest limit of the instruments for scratch hardness (10 kg) and impact resistance (100 cm) as given in Table 13. The nanocomposites also exhibited the lowest limit of the instruments for flexibility evaluation (bending diameter of mandrel is 1 mm) as they possessed high elongation at break.

Table 13 Performance of pristine hyperbranched epoxy and its nanocomposites with MITH-NH

Parameters	TAHE20	MITH-NH1	MITH-NH2	MITH-NH3
Swelling value (%)	24	22	22	21
Tensile strength (MPa)	40±1.0	53.4±1.4	63.5±1.2	72.5±1.5
Elongation at break (%)	21±1.0	27±0.8	43.5±0.5	54.6±1.4
Toughness (MPa)	540	748	1553	2317
Scratch hardness (kg)	9.0±0.5	>10.0	>10.0	>10.0
Impact resistance (cm)	>100	>100	>100	>100
Bending diameter (mm)	<1	<1	<1	<1
Initial degradation temperature (°C)	267	285	288	296

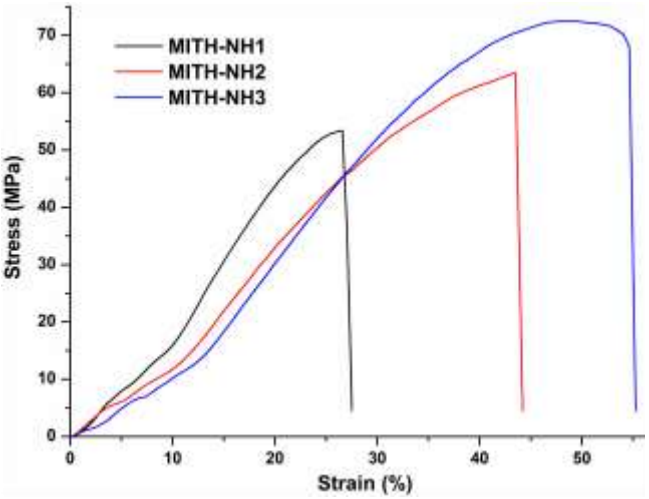

Figure 39 Stress-strain profiles of the nanocomposites

The initial thermal degradation (5% weight loss) temperatures of the pristine thermoset and its nanocomposites are given in Table 13 and TGA curves are shown in Figure 40. From the results it was found that the initial degradation temperature of hyperbranched epoxy thermoset increased up to 30 °C after formation of nanocomposite with 3 wt% MITH-NH nanohybrid. The initial degradation temperature increased with the increase in the amount of nanohybrid loading.

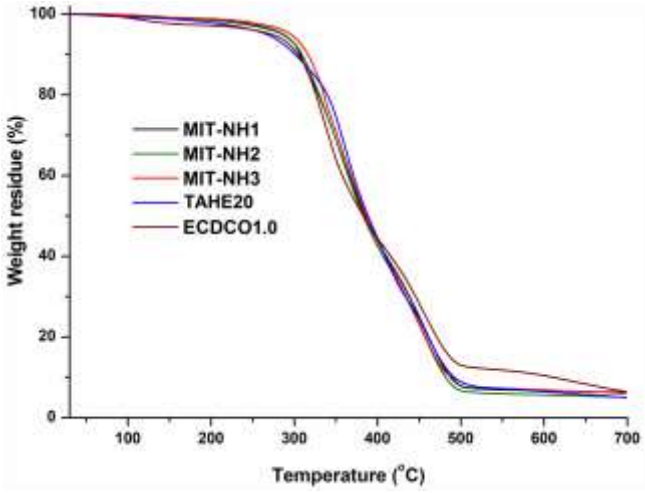

Figure 40 TGA thermograms for pristine hyperbranched epoxy (TAHE20) and its nanocomposites with MITH-NH and carbon dot reduced Cu_2O nanohybrids

Antibacterial test of nanocomposites was done by well diffusion method. Hyperbranched epoxy/ECDCONC nanocomposites showed significant antimicrobial activity towards different gram positive and gram negative bacteria as shown in Figure 41 (a-c). However, they showed poor antifungal activity against Candida albicans as shown in Figure 41d. Whereas MITH immobilized nanocomposites exhibited excellent antifungal and antibacterial activity. The bacterial growth curves for MITH-NH1, MITH-NH2, and MITH-NH3 against gram positive and gram negative bacteria are shown in Figure 42. From the curves it is found that the bacterial growths for all the tested bacteria were completely inhibited by the nanocomposites at high dose of MITH-NH. The zones of inhibition against different bacterial strains are shown in Figure 43. The antifungal activity of the nanocomposites against *Candida albicans* is given in Figure 44. From these figures, it is seen that the nanocomposites formed clear inhibition zones against the tested microbes. The diameter of the zone increases with an increase in the amount of MITH-NH in the nanocomposite and MITH-NH3 shows even larger zone of inhibition than the control. The fungal growth curves of the nanocomposites are shown in Figure 44b. Where, it is seen that MITH-NH3 completely inhibits the fungal growth. Biofilm formation study was done only for TAHE20 and MITH-NH2 against *Candida albicans* fungal strain. The whole antimicrobial study of the nanocomposites was done in dispersed state in DMSO. However the application of the nanocomposites is more important in solid film. So the biofilm formation study was done on the nanocomposite film surface. From the study it was found that greater number of fungus adhered on TAHE20 film compared to MITH-NH2 film as shown in Figure 45. Thus it is confirmed that MITH-NH2 inhibited more fungal adherence on the surface of the film as compared to MITH-NH0 which is due to the presence of MITH as well as Cu_2O nanoparticles on the surface of MITH-NH2 film. The release profile of the biocide from the nanocomposites is shown in Figure 46.

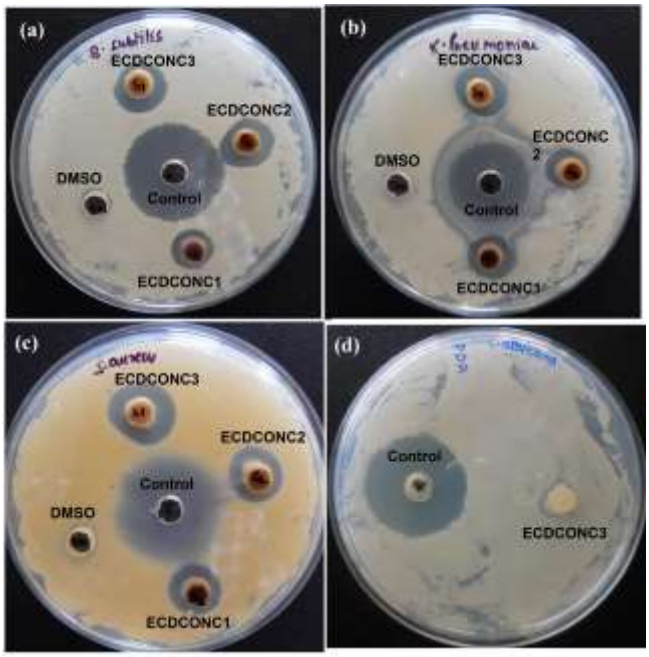

Figure 41 Antimicrobial activity of hyperbranched epoxy nanocomposites with ECDCONC nanohybrid against (a) *Bacillus subtilis*, (b) *Klebsiella pneumonia*, and (c) *Staphylococcus aureus* bacteria; and (d) *Candida albicans* fungus

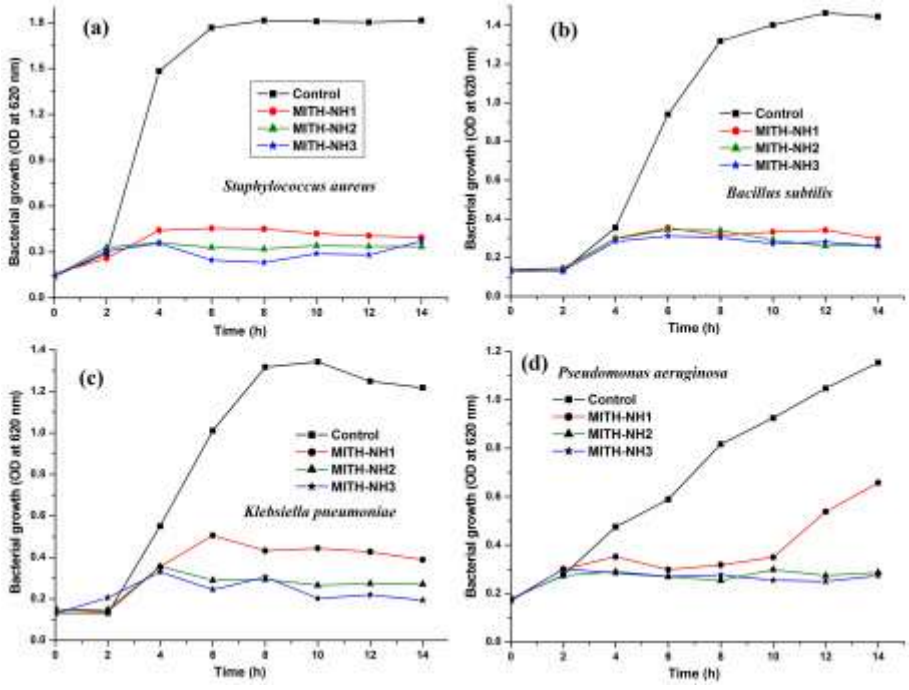

Figure 42 Bacterial growth curves of hyperbranched epoxy nanocomposites with MITH-NH nanohybrid against (a) *Staphylococcus aureus*, (b) *Bacillus subtilis*, (c) *Klebsiella pneumoniae* and (d) *Pseudomonas aeruginosa* bacteria

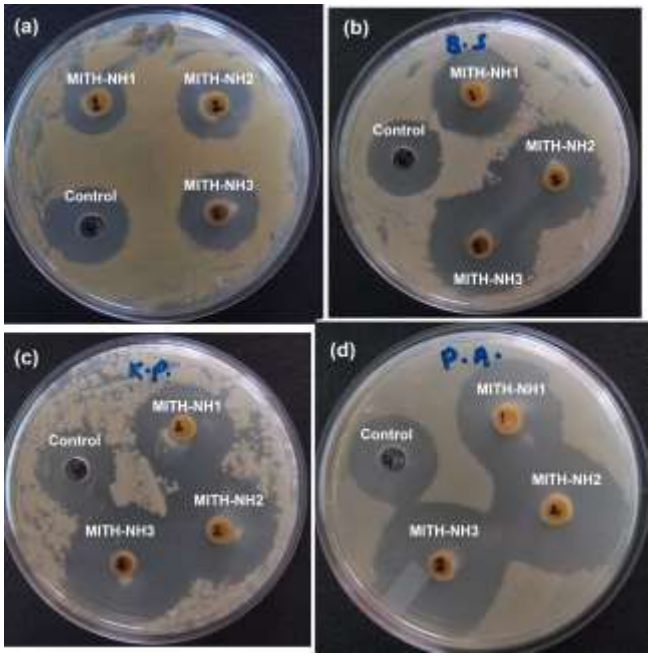

Figure 43 Antibacterial activity of MITH-NH1, MITH-NH2 and MITH-NH3 against (a) *Staphylococcus aureus*, (b) *Bacillus subtilis*, (c) *Klebsiella pneumoniae* and (d) *Pseudomonas aeruginosa* bacteria

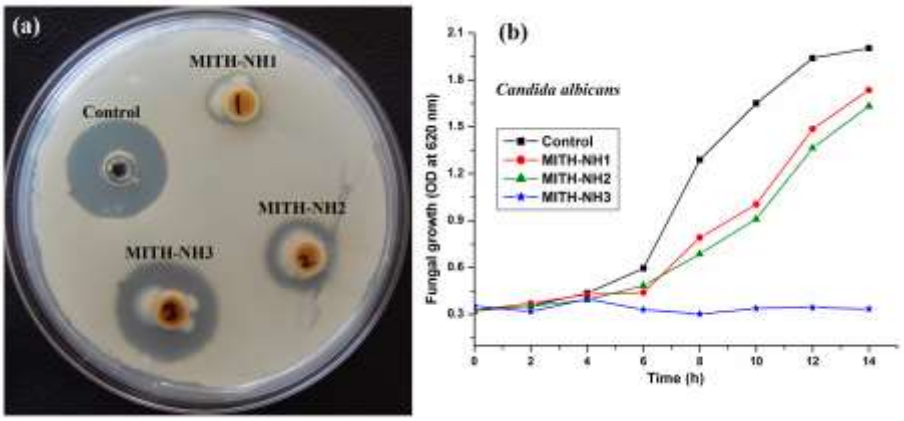

Figure 44 Antifungal activity of MITH-NH1, MITH-NH2 and MITH-NH3 against *Candida albicans*, (a) zone of inhibition and (b) growth curves

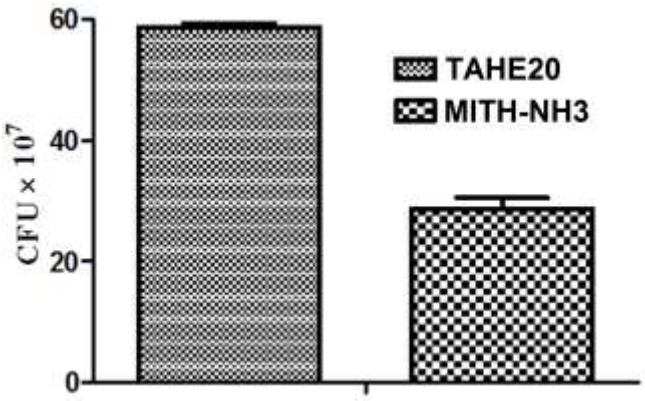

Figure 45 Number of *Candida albicans* adherence on the surface of TAHE20 and MITH-NH2

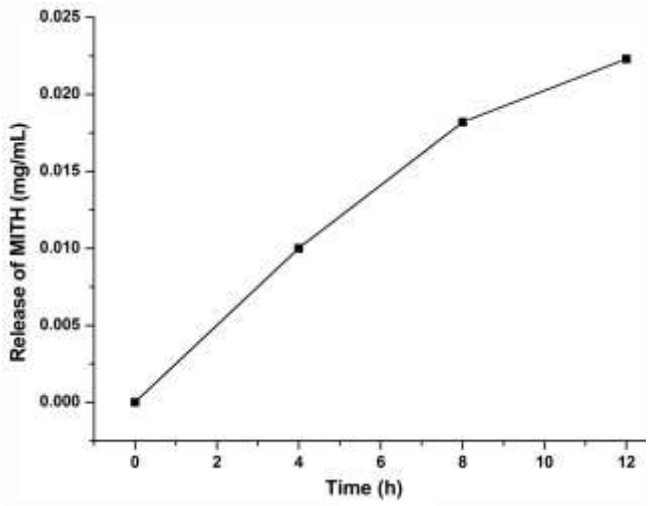

Figure 46 Release profile of MITH biocide for MITH-NH3

NRB work

1. The pristine resin along with the hardener system and the optimized best performing nanocomposite (each 100 g) has been sent to the NRB collaborators for field trial.

Publications

Based on the above results following publications are credited.

In Journal

1. S. Barua, G. Dutta, N. Karak, Glycerol based tough hyperbranched epoxy: Synthesis, statistical optimization and property evaluation, *Chem. Eng. Sci.* **95**, 137-147, 2013. **(Impact factor: 2.61)**

2. S. Barua, R. Konwarh, S. S. Bhattacharya, P. Das, K. S. P. Devi, T. K. Maiti, M. Mandal, N. Karak, Non-hazardous anticancerous and antibacterial colloidal 'green' silver nanoparticles, *Colloids, Surf. B.* **105**, 37-42, 2013. **(Impact factor: 4.28)**

3. S. Barua, G. Das, L. Aidew, A. K. Buragohain, N. Karak, Copper/copper oxide coated nanofibrillar cellulose-a promising biomaterial, *RSC Adv*, **3**, 14997-15004, 2013. **(Impact factor: 3.71)**

4. S. Barua, R. Konwarh, M. Mandal, R. Gopalakrishnan, D. Kumar, N. Karak, Biomimetically prepared antibacterial, free radical scavenging poly(ethylene glycol) supported silver nanoparticles as *Aedes albopictus* larvicide, *Adv. Sci. Eng. Med.* **5**, 1-8, 2013. **(Impact factor: XX)**

5. B. De, N. Karak, Novel high performance tough hyperbranched epoxy by an A_2+ B_3 polycondensation reaction, *J. Mater. Chem. A* **1**, 348-353, 2013. **(Impact factor: XX, J. Mater. Chem. 6.63)**

6. B. De, N. Karak, A green and facile approach for the synthesis of water soluble fluorescent carbon dots from banana juice, *RSC Adv.* **3**, 8286-8290, 2013. **(Impact factor: 3.71)**

7. B De, B Voit, N Karak**,** Transparent Luminescent Hyperbranched Epoxy/Carbon Oxide Dot Nanocomposites with Outstanding Toughness and Ductility, *ACS Appl. Mater. Interfaces* **5**, 10027-10034, 2013. **(Impact factor: 5.90)**

8. B. De, K. Gupta, M. Mandal, N. Karak, Bio-degradable hyperbranched epoxy from castor oil based hyperbranched polyester polyol, *ACS Sustainable Chem. Eng.* **2**, 445−453, 2014. **(Impact factor: XX)**

9. B. De, N. Karak, A room temperature cured low dielectric hyperbranched epoxy adhesive with high mechanical strength, *J. Chem. Sci*. **126**, 587-595, 2014. **(Impact factor: 1.22)**

10. B. De, N. Karak, Tough hyperbranched epoxy/poly(amido-amine) modified bentonite thermosetting nanocomposites, *J. Appl. Polym. Sci*. **131**, 40327 (8 p), 2014. **(Impact factor: 1.60)**

11. B De, B Voit, N Karak, Carbon dot reduced Cu_2O nanohybrid/hyperbranched epoxy nanocomposite: mechanical, thermal and photocatalytic activity, *RSC Adv.* **4**, 58453-58459, 2014. **(Impact factor: 3.71)**

12. B. De, K. Gupta, M. Mandal, N. Karak, Tough hyperbranched epoxy/neem-oil-modified OMMT thermosetting nanocomposite with an antimicrobial attribute, *New J. Chem*. **39**, 595-603, 2015. **(Impact factor: 3.16)**

13. B. De, K. Gupta, M. Mandal, N. Karak, Biocide immobilized OMMT-carbon dot reduced Cu_2O nanohybrid/hyperbranched epoxy nanocomposites: Mechanical, thermal, antimicrobial and optical properties, *Mater. Sci. Eng. C* (Revision submitted) **(Impact factor: 2.74)**

14. S. Barua, N. Dutta, S. Karmakar, P. Chattopadhyay, L. Aidew, A. K. Buragohain, N. Karak, Biocompatible high performance hyperbranched epoxy/clay nanocomposite as an implantable material, *Biomed. Mater.* **9**, 025006, 2014. **(Impact factor: 2.92)**

15. S. Barua, S. Thakur, , L. Aidew, A. K. Buragohain, P. Chattopadhyay, N. Karak, One step preparation of a biocompatible, antimicrobial reduced graphene oxide-silver nanohybrid as a topical antimicrobial agent, *RSC Adv*. **4**, 9777-9783, 2014. **(Impact factor: 3.71)**

16. S. Barua, P. Chattopadhyay, L. Aidew, A. K. Buragohain, N. Karak, Infection resistant hyperbranched epoxy nanocomposite as a scaffold for skin tissue regeneration, *Polym. Int.* **64**, 303–311, 2015.**(Impact factor: 2.24).**

17. S. Barua, P. Chattopadhyay, M.M. Phukan, B.K. Konwar, J. Islam, N. Karak, Biocompatible hyperbranched epoxy/silver–reduced graphene oxide–curcumin nanocomposite as an advanced antimicrobial material, *RSC Adv*. **4**, 47797-47805, 2014. **(Impact factor: 3.71)**

18. S. Barua, P. Chattopadhyay, M.M. Phukan, B.K. Konwar, N. Karak, Hyperbranched epoxy/MWCNT-CuO-nystatin nanocomposite as a high performance, biocompatible, antimicrobial material, *Mater. Res. Express* **1**, pp 045402, 2014. **(Impact factor: XX)**

Conference/seminar/workshop abstract

1. S. Barua, P. Chottapadhyay and N. Karak, Hyperbranched epoxy clay nanocomposite as tissue scaffold material, National conference on health and hygiene (TEZCON-12), Defence Research Laboratory, Tezpur, 6-8 November, 2012.
2. De B. and Karak, N., Hyperbranched epoxy/carbon dots nanocomposites as advanced adhesive materials, International conference on Rubber and Rubber - Like Materials, (ICRRM-2013), IIT Kharagpur, Kharagpur, 6-9 March, 2013.
3. S. Barua, P. Chottapadhyay and N. Karak, Bio-resource based thermostable and cytocompatible micro-crystalline cellulose, 100th Indian science congress, Kolkata, 3-7 January, 2013.
4. S. Barua and N. Karak, 'Carbon nanotube copper oxide nanohybrid immobilized antibiotic as an efficient antimicrobial agent', 3rd International conference on advanced nanomaterials and nanotechnology (ICANN-13), IIT Guwahati, 1-3 December, 2013.
5. S. Barua and N. Karak, Hyperbranched epoxy/clay nanocomposite as an efficient antimicrobial coating material, APA International Conference on Polymers visions and innovations (APA-2014), IIT Delhi, New Delhi, 19-21 February 2014.
6. B. De and N. Karak, Photoluminescent Transparent Hyperbranched Epoxy/Carbon Dot Nanocomposites, APA International Conference on Polymers visions and innovations (APA-2014), IIT Delhi, New Delhi, 19-21 February 2014. **(Awarded as Best Poster)**
7. B. De and N. Karak, Water Soluble Fluorescent Carbon Dot and Its Applications, 3rd International conference on advanced nanomaterials and nanotechnology (ICANN-13), IIT Guwahati, 1-3 December, 2013.

FINAL STATEMENT OF EXPENDITURE

Period of April 2012 –March 2015

NAME OF THE INSTITUE: Tezpur University

NRB Project No.	NRB-251/MAT/11-12	Project Title	Hyperbranched epoxy nanohybrides immobilized natural biocide for advanced marine coatings
Name of Co-ordinator / PI:	Prof. Niranjan Karak	Project Sanction letter no. & date	DNRD/05/4003/NRB/251 dated 29 Feb 12

AUDITED STATEMENT OF ACCOUNT FOR THE PERIOD FROM 1st April, 2012 TO 31st March, 2015

RECEIPT			PAYMENTS					BALANCE
Opening Balance	Receipts	Total	Research Staff /Travel	Equipment/ Consumables	Contingency / Others	Overheads	Total Expenditure	
Rs.	Rs.	Rs.	Rs.	Rs.	Rs.	Rs.	Rs	Rs.
38,31,200/-	38,31,200/-	38,31,200/-	9,11,200/- 1,09,575/-	20,03,588/- 3,01,286/-	1,60,058/-	3,39,200/-	38,24,907/-	6,293/-*

The balance amount is refunded to the funding agent through the draft No.135370.dated.14.05.2015

(i) Certified that the accounts in respect of the funds given by the MOD/Govt. of India have been audited by the C&AG

(ii) Certified that the expenditure from the grant has been audited by this office and it is certified by the Internal Auditor that the grant has been utilized for the purpose for which it was sanctioned.

For SURAJIT CHAKRABORTY & CO.
CHARTERED ACCOUNTANTS

12.05.2015

CA. SURAJIT CHAKRABORTY
(Proprietor)
Membership No.- 305054

Niranjan Karak

Prof. N. Karak
Principal Investigator
Dept. of Chemical Sciences
Tezpur University
Date

Prof. Niranjan Karak
Principal Investigator
Dept. of Chemical Sciences
Tezpur University

Registrar
Tezpur University
Date

Registrar
Tezpur University

30/4/15

Finance Officer
Tezpur University
Date

Finance Officer
Tezpur University

Auditor
Seal
Date

SURAJIT CHAKRABORTY & CO. MRN- 305054 TEZPUR CHARTERED ACCOUNTANT

To

1. The funding through the Co-ordinator
2. The Co-ordinator
3. File copy

FINAL UTILIZATION CERTIFICATE

For the duration of the project: April 2012-March 2015

1	Title of the Project /Scheme	Hyperbranched Epoxy Nanohybrides Immobilized Natural Biocide for Advanced Marine Coatings
2	Name of the Institution	Tezpur University
3	Principal Investigator	Professor Niranjan Karak
4	Naval Research Board Letter No. & Date Sanctioning the project	NRB/251/MAT/11-12 dated 29 Feb. 12
5	Head of account as given in the original sanction order	Research Staff= 9,11,200/- Travel=1,09,575/- Equipment= 20,00,000/- Consumables=3,00,000/- Contingency=1,60,000/- Others= 3,39,200/-
6	Amount Brought forward the previous financial year	Nil
7	Amount received during the project period	Rs. 38,31,200/-
8	Total amount that was available for expenditure (excluding commitments) during the financial year (S. No. 6+7)	Rs. 38,31,200/-
9	Actual expenditure	Rs. 38,24,907/-
10	Balance amount	Rs. 6,293/-
11	Unspent balance refunded if any (Please give details of cheque No. etc.)	Rs. 6,293/-
12	Amount to be carried forward to the next financial year (if applicable)	Not applicable

तेजपुर विश्वविद्यालय
(केंद्रीय विश्वविद्यालय)
नपाम, तेजपुर - 784 028, असम, भारत

TEZPUR UNIVERSITY
(A Central University)
Napam, Tezpur - 784 028, Assam, India

FINAL UTILISATION CERTIFICATE

Certified that out of Rs. **38,31,200/-** of grants-in-aid sanctioned during the project period from **2012-2015** in favour of **Registrar, Tezpur University** under this Ministry of Defence order No **NRB/251/MAT/11-12 dated 29 Feb. 12** and Rs. **38,24,907/-** has been utilized for the purpose of the **project** for which it was sanctioned. The balance amount **Rs. 6,293/-** is refunded to the funding agent through the draft No. 135370 dated 14.05.2015

For SURAJIT CHAKRABORTY & CO.
CHARTERED ACCOUNTANTS
12.05.2015
CA. SURAJIT CHAKRABORTY
(Proprietor)
Membership No.- 305054

Prof. N. Karak	Registrar	Finance Officer	Auditor
Principal Investigator	Tezpur University	Tezpur University	Seal
Date 29/04/15	Date	Date 30/4/15	Date

Prof. Niranjan Karak
Principal Investigator
Dept. of Chemical Sciences
Tezpur University

Registrar
Tezpur University

Finance Officer
Tezpur University

(TO BE FILLED IN NRB)

Certified that I have satisfied myself that the conditions on which the grants in aid was sanctioned have been fulfilled/are being fulfilled and that I have exercised the necessary checks to see that the money was actually utilized for the purpose for which it was sanctioned.

GRANTS-IN-AID SCHEME: NAVAL RESEARCH BOARD
PROFORMA FOR FINAL REPORT OF WORK

- The final report will cover work done during the complete period of the project or from the date of commencement of work to the end of project date of the sanctioned projects

PART 1

1. Name and Designation of Investigator : Dr. Niranjan Karak, Professor

2. Name and Address of Institution : Tezpur University, Tezpur, Assam, India

3. Title of Project : Hyperbranched Epoxy Nanohybrides Immobilized Natural Biocide for Advanced Marine Coatings

4. Reference of Sanction Letter : NRB/251/MAT/11-12 dated 29 Feb. 12

5. Period for which sanctioned : April 2012-March 2015

6. Date of commencement of work : 1st April, 2012
(The project would be deemed to be operative with effect from the date funds are recd by the Institution)

7. Total amount sanctioned :

Year	Research Staff	Equipment Capital	Consumable	Travel (TA/DA)	Contingencies	Others
1st	2,88,000/-	20,00,000/-	1,00,000/-	40,000/-	50,000/-	2,47,800/-
2nd	2,88,000/-	-	1,00,000/-	50,000/-	50,000/-	38,800/-
3rd	3,36,000/-	-	1,00,000/-	30,000/-	60,000/-	52,600/-

8. Statement of accounts certified by competent authority (Likely unspent balance at the time of expiry of the period and the saving made, if any, under different heads should be clearly indicated) ***Please see the final SE as attached***.

Period	Grant Released (under different heads)	Expenditure incurred (under different heads)	Balance (under different heads)	Additional funds required in the following year (under different heads
1	2	3	4	5
	Staff Equipment Consumables TA/DA Contingencies Others: specify			
Total:				

9. Details of staff in position (indicating change, if any)

Year	Designation of Post(s) with pay as sanctioned	Name (s)	Qualifications & Experience	Date of appointment	Date of resignation	Period for which employed
1	2	3	4	5	6	7
2012-15	JRF	Shaswat Barua	M.Sc./4.0 years	1/4/2012	N/A	April 12-March 15
2012-15	JRF	Bibekananda De	M.Sc./4.0 years	1/4/2012	N/A	April 12-March 15

10. Inventory and cost of equipment purchased out of the grant (till date).

Rs. 20,03,588/-

11. Details of visits, seminar, symposia etc attended within the country.

Please see the attached sheet as presentation in conference, seminar, workshop, etc.

Niranjan Karak

Signature of the Principal Investigator

Prof. Niranjan Karak
Principal Investigator
Dept. of Chemical Sciences
Tezpur University

Date: 27/04/15

Signature of Executive Authority of the Institution (Registrar or any other designated officer of the Institution

Registrar
Tezpur University

Name and Designation

12. Certified that the funds received from NRB have not been utilized for any purpose other that what have been clearly indicated in the sanction. None of the staff members who are already receiving salary from the Institution have been paid by remuneration by way of consultancy fees.

Niranjan Karak

Signature of the Principal Investigator

Prof. Niranjan Karak
Principal Investigator
Dept. of Chemical Sciences
Tezpur University

Date: 27/04/15

30/4/15

Signature of the Accounts Officer

Finance Officer
Tezpur University

Date:

Signature of Executive Authority

Registrar
Tezpur University

Date:

PART II

1. (a) Aim of Project : To develop a suitable marine coating

   (b) Key Words :Hypebranched epoxy, Nanocomposite, Biocide

2. Complete resume of all the relevant literature available on work done on subject in India and abroad giving as Appendix A : Given as Appendix A

3. A brief summary of work done and results achieved from the inception of the project till date (only in the case of projects sanctioned prior to the period covered by this progress report). Pl give as Appx B : Given as Appendix B

4. Detailed report of progress of work on the project during the year covered by this report (to be given as a technical report separately) : Attached separately

5. Further programme of work : N/A

6. Number of papers published with titles, name of journal & year of publication (till date) : 18 and 07 presentations

List of publications

1. S. Barua, G. Dutta, N. Karak, Glycerol based tough hyperbranched epoxy: Synthesis, statistical optimization and property evaluation, *Chem. Eng. Sci.* **95**, 137-147, 2013. **(Impact factor: 2.61)**

2. S. Barua, R. Konwarh, S. S. Bhattacharya, P. Das, K. S. P. Devi, T. K. Maiti, M. Mandal, N. Karak, Non-hazardous anticancerous and antibacterial colloidal 'green' silver nanoparticles, *Colloids, Surf. B.* **105**, 37-42, 2013. **(Impact factor: 4.28)**

3. S. Barua, G. Das, L. Aidew, A. K. Buragohain, N. Karak, Copper/copper oxide coated nanofibrillar cellulose-a promising biomaterial, *RSC Adv*, **3**, 14997-15004, 2013. **(Impact factor: 3.71)**

4. S. Barua, R. Konwarh, M. Mandal, R. Gopalakrishnan, D. Kumar, N. Karak, Biomimetically prepared antibacterial, free radical scavenging poly(ethylene glycol) supported silver nanoparticles as *Aedes albopictus* larvicide, *Adv. Sci. Eng. Med.* **5**, 1-8, 2013. **(Impact factor: XX)**

5. B. De, N. Karak, Novel high performance tough hyperbranched epoxy by an A_2+ B_3 polycondensation reaction, *J. Mater. Chem. A* **1**, 348-353, 2013. **(Impact factor: XX, J. Mater. Chem. 6.63)**

6. B. De, N. Karak, A green and facile approach for the synthesis of water soluble fluorescent carbon dots from banana juice, *RSC Adv.* **3**, 8286-8290, 2013. **(Impact factor: 3.71)**

7. B De, B Voit, N Karak**,** Transparent Luminescent Hyperbranched Epoxy/Carbon Oxide Dot Nanocomposites with Outstanding Toughness and Ductility, *ACS Appl. Mater. Interfaces* **5**, 10027-10034, 2013. **(Impact factor: 5.90)**

8. B. De, K. Gupta, M. Mandal, N. Karak, Bio-degradable hyperbranched epoxy from castor oil based hyperbranched polyester polyol, *ACS Sustainable Chem. Eng.* **2**, 445−453, 2014. **(Impact factor: XX)**

9. B. De, N. Karak, A room temperature cured low dielectric hyperbranched epoxy adhesive with high mechanical strength, *J. Chem. Sci*. **126**, 587-595, 2014. **(Impact factor: 1.22)**

10. B. De, N. Karak, Tough hyperbranched epoxy/poly(amido-amine) modified bentonite thermosetting nanocomposites, *J. Appl. Polym. Sci*. **131**, 40327 (8 p), 2014. **(Impact factor: 1.60)**

11. B De, B Voit, N Karak, Carbon dot reduced Cu_2O nanohybrid/hyperbranched epoxy nanocomposite: mechanical, thermal and photocatalytic activity, *RSC Adv.* **4**, 58453-58459, 2014. **(Impact factor: 3.71)**

12. B. De, K. Gupta, M. Mandal, N. Karak, Tough hyperbranched epoxy/neem-oil-modified OMMT thermosetting nanocomposite with an antimicrobial attribute, *New J. Chem*. **39**, 595-603, 2015. **(Impact factor: 3.16)**

13. B. De, K. Gupta, M. Mandal, N. Karak, Biocide immobilized OMMT-carbon dot reduced Cu_2O nanohybrid/hyperbranched epoxy nanocomposites: Mechanical, thermal, antimicrobial and optical properties, *Mater. Sci. Eng. C* (Revision submitted) **(Impact factor: 2.74)**

14. S. Barua, N. Dutta, S. Karmakar, P. Chattopadhyay, L. Aidew, A. K. Buragohain, N. Karak, Biocompatible high performance hyperbranched epoxy/clay nanocomposite as an implantable material, *Biomed. Mater.* **9**, 025006, 2014. **(Impact factor: 2.92)**

15. S. Barua, S. Thakur, , L. Aidew, A. K. Buragohain, P. Chattopadhyay, N. Karak, One step preparation of a biocompatible, antimicrobial reduced graphene oxide-silver nanohybrid as a topical antimicrobial agent, *RSC Adv.* **4**, 9777-9783, 2014. **(Impact factor: 3.71)**

16. S. Barua, P. Chattopadhyay, L. Aidew, A. K. Buragohain, N. Karak, Infection resistant hyperbranched epoxy nanocomposite as a scaffold for skin tissue regeneration, *Polym. Int.* **64**, 303–311, 2015.**(Impact factor: 2.24).**

17. S. Barua, P. Chattopadhyay, M.M. Phukan, B.K. Konwar, J. Islam, N. Karak, Biocompatible hyperbranched epoxy/silver–reduced graphene oxide–curcumin nanocomposite as an advanced antimicrobial material, *RSC Adv*. **4**, 47797-47805, 2014. **(Impact factor: 3.71)**

18. S. Barua, P. Chattopadhyay, M.M. Phukan, B.K. Konwar, N. Karak, Hyperbranched epoxy/MWCNT-CuO-nystatin nanocomposite as a high performance, biocompatible, antimicrobial material, *Mater. Res. Express* **1**, pp 045402, 2014. **(Impact factor: XX)**

Presentation in conference, seminar, workshop, etc.

1. S. Barua, P. Chottapadhyay and N. Karak, Hyperbranched epoxy clay nanocomposite as tissue scaffold material, National conference on health and hygiene (TEZCON-12), Defence Research Laboratory, Tezpur, 6-8 November, 2012.
2. De B. and Karak, N., Hyperbranched epoxy/carbon dots nanocomposites as advanced adhesive materials, International conference on Rubber and Rubber - Like Materials, (ICRRM-2013), IIT Kharagpur, Kharagpur, 6-9 March, 2013.
3. S. Barua, P. Chottapadhyay and N. Karak, Bio-resource based thermostable and cytocompatible micro-crystalline cellulose, 100th Indian science congress, Kolkata, 3-7 January, 2013.

4. S. Barua and N. Karak, 'Carbon nanotube copper oxide nanohybrid immobilized antibiotic as an efficient antimicrobial agent', 3rd International conference on advanced nanomaterials and nanotechnology (ICANN-13), IIT Guwahati, 1-3 December, 2013.
5. S. Barua and N. Karak, Hyperbranched epoxy/clay nanocomposite as an efficient antimicrobial coating material, APA International Conference on Polymers visions and innovations (APA-2014), IIT Delhi, New Delhi, 19-21 February 2014.
6. B. De and N. Karak, Photoluminescent Transparent Hyperbranched Epoxy/Carbon Dot Nanocomposites, APA International Conference on Polymers visions and innovations (APA-2014), IIT Delhi, New Delhi, 19-21 February 2014.
7. B. De and N. Karak, Water Soluble Fluorescent Carbon Dot and Its Applications, 3rd International conference on advanced nanomaterials and nanotechnology (ICANN-13), IIT Guwahati, 1-3 December, 2013.

Niranjan Karak

Signature and name of the Principal Investigator

Date: 22/09/15

Appendix A

Biofouling has been a longstanding trouble associated with the coating materials applied in medical devices, implants, packaging materials, marine equipments etc. Thus, the demand of the hour is to design novel coating materials that would provide fouling preventing surfaces. Toxicity to health and environment is the major issue associated with the prevailing antifouling systems [1].

Polymer nanocomposite is one of the most developed areas in nanotechnology as well as material science. Incorporation of nanoclay into various polymers enhances the properties like mechanical, thermal, physical, barrier, etc. are extensively reported in last two decades [2-6]. High surface area, intercalation chemistry and natural availability of clay make them most popular among all the nanomaterials. They have high tendency to absorb or intercalate different bio-molecules like drugs or biocides, organo-molecules or different nanoparticles between their layered structures and thus recently they are attracted great attention in biological field. However, high moisture absorption and incompatibility with the hydrophobic polymer chains restrain the incorporation of clay particle into the polymer matrix. Thus organically modified clay is significantly used in polymer nanocomposites and this modification can be done either by surface modification or by cation exchange. The modification of clay is mainly performed to create new materials for new or special properties as well as applications. Among the different matrices for fabrication of polymer/clay nanocomposites epoxy resins are extensively used because of their high tensile strength, modulus and stiffness; good thermal stability and chemical resistance [7-11]. They are mainly used as structural materials, coating materials, flooring materials, etc. However, epoxy matrixes possess low toughness and are brittle in nature and incorporation of clay makes them more brittle after formation of nanocomposites. Thus modification of the clay has to be done in such way that it introduces some toughness and flexibility to the epoxy nanocomposite. Phua et al recently reported polyether polyurethane composites, with dopamine-modified nanoclay [12]. Therefore, modification of clay with an available and cost-effective method would be a good proposition. *Homalomena aromatica* (Sugandhmatri) is an important medicinal plant found widely in the forests of Asia and the Southwestern Pacific [13]. The rhizome oil of *H. aromatica* contains about 96.1% total oil, where linalool is the highest component. This oil is well-reported to possess efficient antifungal and insecticidal activity. It was assumed that incorporation of the oil would offer improved compatibility of the nanoclay with the epoxy matrix as well as imparting an antimicrobial effect to the nanocomposite. Again, silver nanoparticles (AgNP) exhibit a broad spectrum antimicrobial activity [14]. Thus, incorporation of silver nanoparticles into the modified clay nanocomposite was expected show resistance to microbial fouling phenomenon. Further, carbon based nanomaterials; like graphene can be considered to anchor silver nanoparticles. Then the nanohybrid can be incorporated to polymeric system to prepare an efficient antifouling coating. However, immobilization of a bio-molecule is further expected to enhance activity of the system. Curcumin (*Curcuma longa*) is a traditionally known molecule to possess tremendous antimicrobial activity [15]. This can be extracted easily from turmeric which is abundantly found in nature. Hence, this was planned to immobilize onto the aforementioned nanohybrid to prepare an antifouling coating material.

Again, antimicrobial polymer nanocomposites are promising materials for surface coating as well as marine industries because of their slow releasing of active agents. Traditionally antimicrobial materials contain one or more toxic compounds like, biocides, metal nanopaticles, etc [16, 17]. However, these materials are associated with the human health as well as environmental problems. In this regard, natural antibiotic immobilized clay reinforced polymer nanocomposite will be preferable which is rarely reported previously. Among the different natural antibiotics, neem seed oil is very common and popular because of its non-toxic effect to mammals as well as a very affective antiseptic, antifungal, antibacterial and insecticidal activity. Crude neem seed oil contains azadirachtin like biocidal compounds as well as long chain fatty acids like linoleic acid, oleic acis, palmitic acid, stearic acid, etc [18]. Thus neem oil will act as an antimicrobial agent as well as the fatty acids of the oil may toughen the whole system by plasticizing effect.

References

1. C. L. Alzieu, J. Sanjuan, J. P. Deltreil, M. Borel, *Pollut. Bull.***1986**, 17, 494.
2. T. Lan and T. J. Pinnavaia, *Chem. Mater.*, **1994**, *6*, 2216.
3. F. Deng and K. J. V. Vliet, *Nanotechnology*, **2011**, *22*, 165703.
4. I. Park, H. Peng, D. W. Gidley, S. Xue and T. J. Pinnavaia, *Chem. Mater.*, **2006**, *18*, 650.
5. J. H.Park and S. C. Jana, *Macromolecules*, **2003**, *36*, 2758.
6. B. Chen, J. R. G. Evans, H. C. Greenwell, P. Boulet, P. V. Coveney, A. A. Bowden and A. Whiting, *Chem. Soc. Rev.*, **2008**, *37*, 568.
7. B. De and N. Karak, *J. Mater. Chem. A*, 2013, **1**, 348.
8. N. Karak, *Fundamentals of Polymers: Raw materials to applications; PHI Learning Pvt. Ltd.*, New Delhi, 2009.
9. J. M. G. Dominguez, A. M. D. Pascual, A. A. Casaos, M. A. G. Fatou and M. T. Martinez, *J. Mater. Chem*., 2011, **21**, 14948.
10. S. Barua, G. Dutta and N. Karak, *Chem. Eng. Sci.*, 2013, **95**, 138.
11. D. Zhang and D. Jia, *J. Appl. Polym. Sci.*, 2006, **101**, 2504.
12. S. L. Phua, L. Yang, C. L. Toh, S. Huang, Z. Tsakadze, S. K. Lau, Y-W Mai and X. Lu, *Appl. Mater. Interfaces* 2012, **4** 4571.
13. G. Singh, I. P. S. Kapoor, O. P. Singh, G. P. Rao, Y. R. Prasad, P. A. Leclercq, N. Klinkby, *Flavour Fragr. J.* 2000, **15** 278.
14. S. Barua, R. Konwarh, M. Mandal, R. Gopalakrishnan, D. Kumar, N. Karak 2013 Biomimetically prepared antibacterial, free radical scavenging poly(ethylene glycol) supported silver nanoparticles as *Aedes albopictus* larvicide, *Adv. Sci. Eng. Med. 2013*, **5,** 201.
15. R. De, P. Kundu, S. Swarnakar, T. Ramamurthy, A. Chowdhury, G. B. Nair, A. K. Mukhopadhyay, *Antimicrob. Agents Chemother*. 2009, **53**, 1592.
16. J. Hrenovic, J. Milenkovic, N. Daneu, R. M. Kepcija and N. Rajic, *Chemosphere*, 2012, **88**, 1103.
17. T. Pongprayoon, R. Nuangchamnong and N. Yanumet, *Appl. Clay Sci*., 2013, **86**, 179.
18. S. Ismadjia, A. Kurniawana, Y.H. Jub, F.E. Soetaredjoa, A. Ayucitraa and L.K. Onga, *Fluid Phase Equilibria*, 2012, **336**, 9.
19. S. Barua, G. Dutta, N. Karak, *Chem. Eng. Sci.*, 2013, **95** 138.
20. S Barua, S Thakur, L Aidew, AK Buragohain, P Chattopadhyay, N Karak, *RSC Adv*., 2014,**4**, 9777.

Appendix B

Executive Summary of achievements of the project

1. Hyperbranched epoxy resins were synthesized by using triethanol amine, glycerol etc. by reacting with bisphenol-A and epichlorohydrin.

2. Curing behavior of the synthesized resins was studied by using polyamine hardener system.

3. Hyperbranched epoxy nanocomposites were prepared by using different nanomaterials like nanoclay, silver nanoparticles decorated nanoclay, Cu-oxides, carbon dot, carbon dot reduced Cu_2O nanohybrid, silver-reduced graphene oxide, copper oxide-carbon nanotubes etc.

4. Immobilization of natural biocide such as neem oil, curcumin, *H. aromatica* oil as well as synthetic ones such as nystatin, MITH etc. were done for attaining antifouling attributes.

5. Detailed characterization of the biocides immobilized nanocomposites has been carried out by using different advanced characterization methods.

6. Performance study of the biocide immobilized nanocomposites as coating materials is carried out. Some preliminary investigations are performed in this regard by testing the biocidal property of the nanocomposite systems against bacteria, fungi and microalgae.

7. The pristine resin along with the hardener system and the optimized best performing nanocomposite (each 100 g) has been sent to the NRB collaborators for field trial.

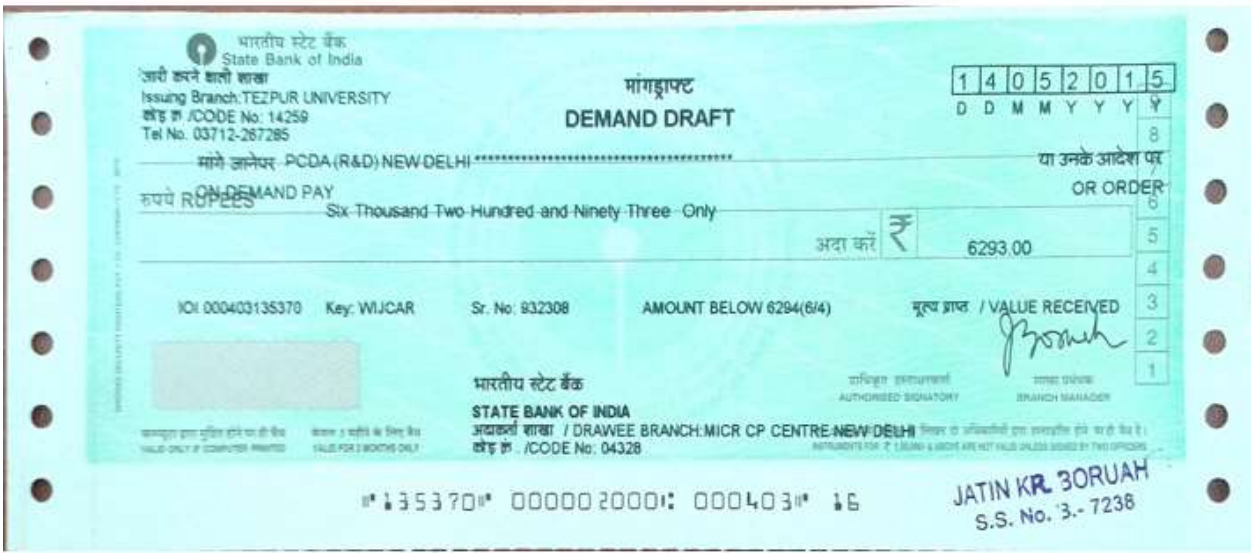

भारतीय स्टेट बैंक
State Bank of India

जारी करने वाली शाखा
Issuing Branch:TEZPUR UNIVERSITY
कोड सं /CODE No: 14259
Tel No. 03712-267285

मांगड्राफ्ट
DEMAND DRAFT

14 05 2015
D D M M Y Y Y Y

माँगे जानेपर PCDA (R&D) NEW DELHI ..... या उनके आदेश पर
ON DEMAND PAY OR ORDER

रुपये RUPEES Six Thousand Two Hundred and Ninety Three Only

अदा करें ₹ 6293.00

IOI 000403135370 Key: WIJCAR Sr. No: 932308 AMOUNT BELOW 6294(6/4) मूल्य प्राप्त / VALUE RECEIVED

भारतीय स्टेट बैंक
STATE BANK OF INDIA
अदाकर्ता शाखा / DRAWEE BRANCH:MICR CP CENTRE NEW DELHI
कोड सं /CODE No: 04328

AUTHORISED SIGNATORY BRANCH MANAGER

JATIN KR. BORUAH
S.S. No. 3.- 7238